Two-Timescale Design for Movable Antennas Enabled-Multiuser MIMO Systems

Ziyuan Zheng, Qingqing Wu, Wen Chen, and Guojie Hu

Abstract-Movable antennas (MAs), which can be swiftly repositioned within a defined region, offer a promising solution to the limitations of fixed-position antennas (FPAs) in adapting to spatial variations in wireless channels, thereby improving channel conditions and communication between transceivers. However, frequent MA position adjustments based on instantaneous channel state information (CSI) incur high operational complexity, making real-time CSI acquisition impractical, especially in fastfading channels. To address these challenges, we propose a two-timescale transmission framework for MA-enabled multiuser multiple-input-multiple-output (MU-MIMO) systems. In the large timescale, statistical CSI is exploited to optimize MA positions for long-term ergodic performance, whereas, in the small timescale, beamforming vectors are designed using instantaneous CSI to handle short-term channel fluctuations. Within this new framework, we analyze the ergodic sum rate and develop efficient MA position optimization algorithms for both maximum-ratiotransmission (MRT) and zero-forcing (ZF) beamforming schemes. These algorithms employ alternating optimization (AO), successive convex approximation (SCA), and majorization-minimization (MM) techniques, iteratively optimizing antenna positions and refining surrogate functions that approximate the ergodic sum rate. Numerical results show significant ergodic sum rate gains with the proposed two-timescale MA design over conventional FPA systems, particularly under moderate to strong line-of-sight (LoS) conditions. Notably, MA with ZF beamforming consistently outperforms MA with MRT, highlighting the synergy between beamforming and MAs for superior interference management in environments with moderate Rician factors and high user density, while MA with MRT can offer a simplified alternative to complex beamforming designs in strong LoS conditions.

Index Terms—Movable antenna, antenna position optimization, ergodic sum rate, two-timescale design.

I. INTRODUCTION

Multiple-input multiple-output (MIMO) has been established as a critical enabler for enhancing capacity, reliability, and overall performance in the evolution of wireless communication systems [1]. MIMO systems provide significant gains in beamforming, spatial multiplexing, and diversity by leveraging independent or quasi-independent channel fading. These gains enable the simultaneous transmission of multiple data streams, significantly boosting spectral efficiency compared to single-antenna systems [2], [3]. As wireless networks transition to higher frequency bands such as millimeter-wave and terahertz, massive MIMO has become crucial for mitigating propagation loss through large-scale antenna arrays and achieving near-orthogonal user channels, thereby improving spectral efficiency and link reliability significantly [4], [5], [6]. Compared to traditional MIMO, massive MIMO's ability to harness

spatial correlation for array gains and interference mitigation renders it essential for next-generation wireless systems.

However, deploying large-scale antenna arrays introduces several challenges, particularly for escalating hardware costs and increased radio-frequency (RF) energy consumption, which hinder the development of sustainable and energyefficient networks [7], [8]. With the advancement towards 6G networks, the limitations of traditional fixed-position antennas (FPAs) become increasingly evident. Due to their stationary nature, FPAs cannot fully leverage spatial variations in wireless channels. To compensate, conventional MIMO and massive MIMO systems resort to increasing the number of antennas and RF chains. While this approach enhances service quality, it comes at the expense of increased energy consumption and hardware cost. Fundamentally, the static nature of FPAs renders them less adaptable to dynamic channel conditions and user distributions, leading to suboptimal performance and constraining their ability to fully exploit spatial diversity and multiplexing [9], [10].

Movable antennas (MAs) [11], also referred to as fluid antennas [12], overcome the limitations of FPAs by enabling flexible positioning within a spatial region. Connected to the RF chain via flexible cables and controlled by drivers. MAs can be swiftly positioned at locations with favorable channel conditions to reshape wireless channels and optimize communication between transceivers. This flexibility allows MAs to exploit spatial degrees of freedom, avoiding deep fading or interference-prone areas without the need for additional antennas or RF chains. By dynamically adjusting antenna positions in response to channel conditions and user distribution, MAs can fully exploit spatial diversity to maximize channel gain, thereby enhancing signal-to-noise ratio (SNR) [13]. MAs also enhance interference mitigation by moving to locations with deep fading relative to interference sources, boosting signal-to-interference-plus-noise ratio (SINR) without requiring multiple antennas [14]. Additionally, MA-enabled MIMO systems optimize spatial multiplexing rates by dynamically adjusting antenna positions to reshape the channel matrix, thus maximizing MIMO capacity [15].

The inherent advantages of MAs make them a promising candidate for integration into 6G networks, sparking significant interest in their deployment across various wireless communication systems, particularly in optimizing antenna positioning. Early research primarily focused on point-to-point single-user systems. In [14], a mechanical MA architecture was proposed within a single-input single-output (SISO) system to enhance SNR gains, which were found to be highly dependent on the number of channel paths and the movement range of the antennas. This concept was later extended to point-to-point MIMO systems in [15], where an alternating

Z. Zheng, Q. Wu, and W. Chen is with the Department of Electronic Engineering, Shanghai Jiao Tong University, 200240, China (e-mail: zhengziyuan2024@sjtu.edu.cn, qingqingwu@sjtu.edu.cn, wenchen@sjtu.edu.cn).

G. Hu is with the Rocket Force University of Engineering, Xi'an, 710025, China (e-mail: lgdxhgj@sina.com).

optimization (AO) algorithm was employed to jointly optimize the positions of MAs and the transmit signal covariance, thereby maximizing channel capacity. Besides point-to-point systems, the application of MAs has been investigated in various multiuser scenarios [16], [17]. Several suboptimal algorithms have been proposed for uplink transmissions involving multiple single-MA users communicating with a base station (BS) equipped with an FPA array. Projected gradient descent techniques were utilized to minimize user transmit power while guaranteeing quality of service [18]. Moreover, particle swarm optimization was applied to improve user fairness for adjusting MA positions and users' transmit power, showcasing the capability of MAs to manage multiuser interference effectively [19]. Downlink scenarios have also been investigated [20]-[25]. For example, integrating sub-connected MAs with hybrid beamforming schemes outperformed fully connected FPA arrays in terms of achievable sum rates under certain conditions [20]. This integration, alongside other studies [14], demonstrated that even minor movements of MAs (within sub-wavelength distances) can substantially alter channel conditions due to small-scale fading, leading to enhanced communication performance. Recent research further indicates that MAs can be effectively applied in multi-cell MISO [22], multi-group multicast [23], full-duplex communications [24], and wideband systems [25].

Despite the promising potential of MA technology, research in this field remains in its early stage, with most studies focusing on algorithmic design and theoretical performance limits. These studies generally assume that each antenna element can be adjusted globally and in real-time within the transmit/receive region, relying on the availability of instantaneous channel state information (CSI) [26]. However, such an approach presents several critical challenges. First, although mechanical MA systems, as discussed in [16] and [17], provide flexible movement in 2D and 3D spaces, this flexibility incurs substantial movement energy consumption due to the need for frequent adjustments to track optimal positions, compounded by delays resulting from mechanical response speed limitations. In contrast, fluid antenna systems (FAS), as studied in [12], [13], [27], are more compact and energy-efficient; however, their movement is confined to 1D spaces, limiting their adaptability in dynamic environments. Second, the reliance on complete and instantaneous CSI across the movement region to optimize MA positions poses an additional fundamental challenge. Most existing schemes rely on full CSI; however, acquiring accurate real-time CSI across the entire movement region is impractical and even infeasible, especially in fast-fading channels. This limitation hinders the practical deployment of MAs in real-world systems.

To address these challenges, an approach that involves adjusting antenna positions on a longer timescale is proposed by utilizing statistical CSI, such as user signal power, user distribution, and large-scale channel parameters, in accordance with current network protocols [28]. This method reduces the overhead and complexity associated with channel estimation while still providing performance gains over traditional FPAs. Another similar research explored scenarios where only statistical CSI is available, proposing simplified antenna

movement modes and optimization frameworks that focus on transmit precoding and antenna position design [29]. However, relying exclusively on statistical CSI can result in performance degradation [30], [31], as it fails to account for rapidly changing channel conditions, especially in multi-path or highly dynamic environments. Therefore, it is imperative to develop a general optimization framework that balances performance improvements with practical implementation challenges in MA-enabled systems.

In this paper, we propose a novel two-timescale transmission framework for MA-enabled multiuser MIMO (MU-MIMO) systems. The key contributions are summarized as follows:

- We propose a two-timescale transmission scheme for MA-enabled systems. The large-timescale optimization exploits statistical CSI to determine optimal MA positions, maximizing long-term ergodic performance, while in the small timescale, beamforming vectors are derived from instantaneous CSI to adapt to short-term channel fluctuations. This decoupling of MA position optimization from the instantaneous transmission process provides a solution that strikes a balance between performance and practicality, reducing the frequency of MA updates and lowering channel estimation overhead.
- 2) Within the proposed two-timescale framework, we analyze the ergodic sum rate under maximum-ratio-transmission (MRT) beamforming and develop an efficient antenna position optimization algorithm. This algorithm employs alternating optimization (AO) and successive convex approximation (SCA) techniques to iteratively optimize MAs' positions in an element-wise manner, enhancing the system's ergodic performance.
- 3) We further extend our analysis to zero-forcing (ZF) beamforming and propose an algorithm that resorts to AO, SCA, and majorization-minimization (MM) techniques. This iterative approach optimizes a surrogate function, which serves as a lower bound for the ergodic sum rate, to refine the antenna positions for enhanced performance.
- 4) Numerical results verify the superiority of the proposed two-timescale MA design compared to conventional FPA systems, indicating considerable ergodic sum rate improvements under moderate to strong line-of-sight (LoS) conditions. Notably, MA combined with ZF beamforming consistently outperforms MA with MRT beamforming, underscoring the synergy between beamforming and MA techniques for superior interference management, especially in environments with moderate Rician factors and high user density. In contrast, MA with MRT beamforming offers a simplified alternative to sophisticated beamforming designs in strong LoS conditions.

The rest of the paper is structured as follows: Section II introduces the system model and problem formulation. Section III presents the achievable rate derivation and antenna position optimization under MRT beamforming. Section IV derives the achievable rate and optimizes MAs' positions under ZF beamforming. Section V presents the numerical results, and Section VI concludes the paper.

Notations: Scalars are denoted by italic letters, and vectors and matrices are denoted by bold-face lower and upper-case

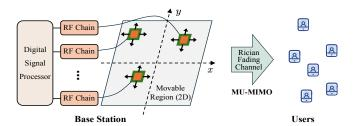


Fig. 1. Illustration of an MA-enabled multiuser system.

letters, respectively. $\mathbb{C}^{x \times y}$ denotes the space of complex matrices. |x| denotes the modulus of a complex-valued scalar x. For a vector \boldsymbol{x} , $\|\boldsymbol{x}\|$ denotes its Euclidean norm and \boldsymbol{x}^{\dagger} denotes its conjugate. The distribution of a circularly symmetric complex Gaussian random vector with mean vector \boldsymbol{x} and covariance matrix $\boldsymbol{\Sigma}$ is denoted by $\mathcal{CN}\left(\boldsymbol{x},\boldsymbol{\Sigma}\right)$. The Euclidean gradient of a scalar function $f(\boldsymbol{x})$ with a vector variable \boldsymbol{x} is denoted by $\nabla f(\boldsymbol{x})$. For a square matrix \boldsymbol{S} , $\operatorname{tr}\left(\boldsymbol{S}\right)$ denote its trace. For any general matrix, \boldsymbol{M}^H and $[\boldsymbol{M}]_{ij}$ denote its conjugate transpose and (i,j)th element,respectively. \boldsymbol{I} denotes an identity matrix, respectively. $\mathbb{E}[\cdot]$ stands for the expectation operation.

II. SYSTEM MODEL AND PROBLEM FORMULATION

A. MA-enabled MU-MIMO System

As shown in Fig. 1, we consider a downlink MU-MIMO system enabled by MAs, where a BS equipped with N transmit MAs serves M single-antenna users. The MAs are connected to RF chains via flexible cables, which allows them to move freely within a designated local region A [16], [17]. Without loss of generality, we assume A a 2D square moving region of size $A \times A$. The position of the n-th transmit MA at the BS is represented by $t_n = [x_n, y_n]^T$, and we define the set of positions as $t \triangleq \{t_n\}$. The reference point of the region \mathcal{A} is represented by $o = [0, 0]^T$. The size of MAs' movement region is significantly smaller than the signal propagation distance, ensuring that the far-field condition holds between the BS and the users. In this configuration, altering the positions of the MAs affects only the phase of the complex channel coefficients for each channel path component without influencing the angle of departure (AoD), angle of arrival (AoA), or the amplitude of the channel gain.

The equivalent baseband channel from the BS to m-th user is denoted as $\boldsymbol{h}_m(\boldsymbol{t}) \in \mathbb{C}^{N \times 1}$, characterized by the general Rician fading model

$$\boldsymbol{h}_{m}(\boldsymbol{t}) = \sqrt{\frac{\kappa_{m}\beta_{m}}{\kappa_{m}+1}} \bar{\boldsymbol{h}}_{m}(\boldsymbol{t}) + \sqrt{\frac{\beta_{m}}{\kappa_{m}+1}} \tilde{\boldsymbol{h}}_{m}(\boldsymbol{t}), \quad (1)$$

where $\kappa_m \geq 0$ is the Rician factor, β_m represents the large-scale fading coefficient, $\bar{h}_m(t) \in \mathbb{C}^{N \times 1}$ denotes the deterministic LoS component, and $\tilde{h}_m(t) \in \mathbb{C}^{N \times 1}$ represents the random non-line-of-sight (NLoS) component. Specifically, the entries of \tilde{h}_m are independent and identically distributed (i.i.d) circularly symmetric complex Gaussian random variables with zero mean and unit variance. To describe the LoS component, let $\theta_m \in \left[-\frac{\pi}{2}, \frac{\pi}{2}\right]$ and $\phi_m \in \left[-\frac{\pi}{2}, \frac{\pi}{2}\right]$ represent the elevation and azimuth AoDs for user m, respectively. The propagation distance difference of the LoS path between the MA position t and the reference position o is given by

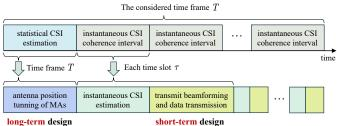


Fig. 2. Illustration of the proposed two-timescale framework.

 $\boldsymbol{t}_n^T \left[\cos\theta_m \sin\phi_m, \sin\theta_m\right]^T \triangleq \boldsymbol{t}_n^T \boldsymbol{a}_m$, and the phase difference of the LoS path is $\frac{2\pi}{\lambda} \boldsymbol{t}_n^T \boldsymbol{a}_m$, with λ denoting the carrier wavelength. Thus, the channel vector of the LoS component between the BS and m-th user can be expressed as

$$\bar{\boldsymbol{h}}_{m}\left(\boldsymbol{t}\right) = \left[e^{j\frac{2\pi}{\lambda}\boldsymbol{t}_{1}^{T}\boldsymbol{a}_{m}}, \dots, e^{j\frac{2\pi}{\lambda}\boldsymbol{t}_{N}^{T}\boldsymbol{a}_{m}}\right]^{T}.$$
 (2)

Let $W = [w_1, w_2, \cdots, w_M] \in \mathbb{C}^{N \times M}$ denote the linear precoding matrix at the BS, where each user is assigned a dedicated beamforming vector. The baseband transmitted signal is given by Ws, where $s = [s_1, \cdots, s_M]^T$ is the data vector, with each element s_m being an independent variable with zero mean and normalized power. The received signal at user m can be expressed as

$$u_m = \boldsymbol{h}_m(\boldsymbol{t})^H \boldsymbol{w}_m s_m + \sum_{j=1, j \neq m}^M \boldsymbol{h}_m(\boldsymbol{t})^H \boldsymbol{w}_j s_j + z_m, \quad (3)$$

where $z_m \sim \mathcal{CN}\left(0, \sigma_m^2\right)$ represents the additive white Gaussian noise (AWGN) at the receiver of user m. Accordingly, the SINR at user m is given by

$$\gamma_m = \frac{\left| \boldsymbol{h}_m(\boldsymbol{t})^H \boldsymbol{w}_m \right|^2}{\sum_{j=1, j \neq m}^M \left| \boldsymbol{h}_m(\boldsymbol{t})^H \boldsymbol{w}_j \right|^2 + \sigma_m^2}.$$
 (4)

The sum achievable rate for all users is then expressed as

$$R = \sum_{m=1}^{M} R_m \triangleq \sum_{m=1}^{M} \log_2 (1 + \gamma_m).$$
 (5)

The sum rate R of the MA-enabled downlink MU-MIMO system in (5) depends on the positions of the transmit MAs t, which affect the BS-user channel $h_m(t)$ as well as the corresponding transmit beamforming matrix W.

B. Two-Timescale Transmission Scheme

In the Rician fading channel $h_m(t)$, the NLoS component $\tilde{h}_m(t)$ is random and varies with different antenna positions at the BS. Estimating all $\{\tilde{h}_m(t)\}_{m=1}^M$ for arbitrary t would require the MA to traverse the entire feasible antenna region, making instantaneous CSI acquisition across the entire region impractical. In contrast, the LoS component in Rician fading channels remains relatively stable, primarily determined by spatial angles and position information. Additionally, large-scale path-loss coefficients and the Rician factor are static over a certain period, making them well-suited for statistical characterization. These properties allow for the optimization of antenna positions using statistical CSI, significantly reducing the overhead associated with real-time CSI estimation.

Building on this insight, we propose a hierarchical twotimescale transmission scheme, as shown in Fig. 2. In the first stage, the antenna positions at the BS are optimized based on statistical CSI, leveraging the stability of the LoS component to enhance long-term system performance. Once the optimal antenna positions are determined and fixed, the system transitions to the small timescale phase, where instantaneous CSI is acquired using conventional channel estimation techniques in multiple-antenna systems. This instantaneous CSI is then used to design the downlink beamforming, ensuring that the dynamic NLoS channel fluctuations are addressed in real time.

Compared to schemes requiring continuous MA repositioning based on instantaneous CSI, our two-timescale design effectively reduces the update frequency of MAs' positions, lowering channel estimation overhead and movement energy consumption. This is particularly beneficial in environments with rapid NLoS fluctuations, where real-time MA adjustments are impractical. By integrating the NLoS component into the beamforming process after antenna positions are fixed, our method preserves the performance gains from this random component, combining the advantages of both statistical and instantaneous CSI. This two-timescale approach thus strikes an effective balance between practicality and performance.

C. Problem Formulation

Under the proposed two-timescale transmission framework, the objective is to maximize the ergodic sum rate for all users by jointly optimizing the antenna positions $\{t_n\}$ in the large timescale and transmit beamforming vectors $\{w_m\}$ in the small timescale at the BS. This leads to the formulation of a general optimization problem as follows

(P1):
$$\max_{\{\boldsymbol{t}_n\}} \mathbb{E}\left[\max_{\{\boldsymbol{w}_m\}} \sum_{m=1}^{M} \log_2 (1 + \gamma_m)\right]$$
 (6a)

s.t.
$$\sum_{m=1}^{M} \|\mathbf{w}_m\|^2 \le P_{\text{tot}},$$
 (6b)

$$\|\boldsymbol{t}_n - \boldsymbol{t}_i\| \ge D_{\min}, \forall n, i \in \mathcal{N}, i \ne n,$$
 (6c)

$$t_n \in \mathcal{C}, \forall n \in \mathcal{N},$$
 (6d)

where $\mathbb{E}\left[\cdot\right]$ in (6a) represents the expectation over all possible channel realizations, $P_{\text{tot}} \geq 0$ in (6b) denotes the maximum transmit power of the BS, (6c) ensures a minimum separation distance between any two adjacent MAs to avoid coupling effects, and (6d) specifies the feasible region for MAs' positions.

Solving (P1) presents significant challenges due to the following reasons: 1. the long-term antenna positions variables $\{t_n\}$ and short-term transmit beamforming variables $\{w_m\}$ are intertwined in the objective function; and 2. the ergodic sum rate lacks a closed-form expression, especially with an unfixed set of antenna positions t_n . Generally, there exists no efficient method to solve this non-convex problem optimally. For the general multiuser case, a stochastic optimization framework similar to the one in [32] can be employed to approximate the solution using randomly generated channel samples. However, this method incurs high computational complexity depending on the scale of the channel samples.

Motivated by these observations, in the following two sections, we investigate the transmission designs for two classical beamforming schemes, namely MRT beamforming and ZF beamforming, in the context of (P1), respectively. For each

scheme, we first derive the achievable rate expression and then propose an efficient algorithm for optimizing the antenna positions, followed by computational complexity analysis.

III. ACHIEVABLE RATE DERIVATION AND ANTENNA POSITION OPTIMIZATION UNDER MRT BEAMFORMING

In this section, within the proposed two-timescale scheme, we derive a closed-form expression for the approximate ergodic rate, leveraging statistical CSI and the structure of small-timescale MRT beamforming under a fixed power allocation strategy. Then, using these expressions and resorting to AO and SCA techniques, we develop an iterative algorithm for antenna position optimization. The analysis and design are extended to ZF beamforming in Section IV.

A. Ergodic Rate Analysis with MRT beamforming

The MRT precoding vector, assuming perfect knowledge of the instantaneous CSI, is expressed as

$$\boldsymbol{w}_{\mathrm{MRT},m} = \sqrt{p_m} \boldsymbol{h}_m \left(\boldsymbol{t} \right), \tag{7}$$

where p_m represents the power allocation parameter, determined to satisfy the total beam power constraint

$$\sum_{m=1}^{M} \|\boldsymbol{w}_{\text{MRT},m}\left(\boldsymbol{t}\right)\|^{2} \triangleq \sum_{m=1}^{M} p_{m} \|\boldsymbol{h}_{m}\left(\boldsymbol{t}\right)\|^{2} \leq P_{\text{tot}}.$$
 (8)

The SINR for MRT beamforming is then given by

$$\gamma_{\text{MRT},m} = \frac{p_m \|\boldsymbol{h}_m(\boldsymbol{t})\|^4}{\sum_{j=1, j \neq m}^{M} p_j \left|\boldsymbol{h}_j^H(\boldsymbol{t}) \boldsymbol{h}_m(\boldsymbol{t})\right|^2 + \sigma_m^2}.$$
 (9)

Note that MRT beamforming aligns conjugate vectors with the corresponding BS-user channels, followed by power allocation¹. To underscore the potential of MA and its position optimization, we simplify the power allocation process to a fixed scheme by setting it proportional to the channel gain between the BS and each user, as follows

$$p_m = p \triangleq \frac{P_{\text{tot}}}{\sum_{m=1}^{M} \|\boldsymbol{h}_m(\boldsymbol{t})\|^2}.$$
 (10)

With MRT beamforming, the antenna position optimization problem for ergodic sum rate maximization can be recast as

$$(P2): \max_{\{\boldsymbol{t}_n\}} \mathbb{E}\left[\log_2\left(1+\gamma_{\mathsf{MRT},m}\right)\right]$$
 s.t. (6c), (6d).

Based on the approximation in [33, Lemma 1], the ergodic rate for user m under statistical CSI is expressed as

$$\mathbb{E}\left\{\log_{2}\left(1+\gamma_{\mathrm{MRT},m}\right)\right\} \approx \log_{2}\left(1+\frac{\mathbb{E}\left\{\left\|\boldsymbol{h}_{m}\left(\boldsymbol{t}\right)\right\|^{4}\right\}}{\mathbb{E}\left\{\sum_{j=1,j\neq m}^{M}\left|\boldsymbol{h}_{j}^{H}\left(\boldsymbol{t}\right)\boldsymbol{h}_{m}\left(\boldsymbol{t}\right)\right|^{2}\right\}+\mathbb{E}\left\{\frac{\sigma_{m}^{2}}{p}\right\}}\right) \triangleq R_{\mathrm{MRT},m}^{app}.$$
(12)

This approximation lies between the upper and lower bounds of $\mathbb{E}\{\log_2(1+\gamma_{MRT,m})\}$. After calculating the expectation terms, we arrive at (13) provided at the top of the next page.

¹In the two-timescale MA transmission scheme, power allocation can also be optimized based on statistical CSI in the large timescale. However, due to limited gains relative to the added complexity, the joint power allocation and antenna position optimization are left for our future work.

$$R_{\text{MRT},m}^{app} = \log_2 \left(1 + \frac{\beta_m^2 \left(\frac{2N\kappa_m + N}{(\kappa_m + 1)^2} + N^2 \right)}{\sum_{j=1, j \neq m}^M \beta_m \beta_j \frac{\kappa_m \kappa_j |\bar{\mathbf{h}}_j(t)\bar{\mathbf{h}}_m^H(t)|^2 + N(\kappa_m + \kappa_j + 1)}{(\kappa_m + 1)(\kappa_j + 1)} + \frac{\sigma_m^2}{P} N \sum_{m=1}^M \beta_m} \right).$$
 (13)

$$R_{\text{MRT},m}^{app}(\boldsymbol{t}_{n}) = \log_{2} \left(1 + \frac{c_{2,m}}{2 \sum_{j=1, j \neq m}^{M} c_{1,m,j} \left| \tau_{n,m,j} \right| \cos \left(\frac{2\pi}{\lambda} \boldsymbol{t}_{n}^{T} \boldsymbol{a}_{m,j} - \angle \tau_{n,m,j} \right) + c_{3,m}} \right), \tag{15}$$

Remark 1: From (13), we can draw three key insights. First, under MRT beamforming in the two-timescale design, MA does not yield any ergodic rate gain through antenna position tuning when M=1, as such gain stems from interference mitigation or channel decorrelation between $\bar{h}_j(t)$ and $\bar{h}_m^H(t)$, $\forall j \neq m$. Second, with $\kappa_m=0$ in the Rician fading channel, the absence of a deterministic LoS component will render MA ineffective in reshaping the channel since the summation term in the denominator of (13) vanishes, and thus $R_{\text{MRT},m}^{app}$ no longer related to t. Third, as the number of antennas N becomes asymptotically large, i.e., $N \to \infty$, the performance gain of MA diminishes due to the channel hardening, where FPAs already achieve asymptotically orthogonal channels for different users, i.e., $\left|\frac{1}{N}\bar{h}_j(t_{\text{FPA}})\bar{h}_m^H(t_{\text{FPA}})\right|^2 \to 0, \forall j,m$.

B. Antenna Position Optimization Based on AO Method

Although we obtain the closed-form expression (13), MAs' positions remain intricately coupled in the non-convex term $|\bar{\boldsymbol{h}}_{j}\left(t\right)\bar{\boldsymbol{h}}_{m}^{H}\left(t\right)|^{2}$ relying on the LoS components. The non-convex minimum distance constraint (6c) further complicates the problem (P2), making it challenging to solve directly.

To address this challenge, we propose an antenna-wise position optimization framework based on the AO method. In this framework, we first derive a tractable expression for the achievable rate concerning the n-th antenna while keeping the positions of the other antennas fixed. Focusing on the n-th antenna, we can express the critical term $\left|\bar{\boldsymbol{h}}_{j}\left(t\right)\bar{\boldsymbol{h}}_{m}^{H}\left(t\right)\right|^{2}=\left|\sum_{n=1}^{N}e^{j\frac{2\pi}{\lambda}\boldsymbol{t}_{n}^{T}\left(\boldsymbol{a}_{m}-\boldsymbol{a}_{j}\right)}\right|^{2}$ as

$$\begin{split} & \left| \bar{\boldsymbol{h}}_{j} \left(\boldsymbol{t}_{n} \right) \bar{\boldsymbol{h}}_{m}^{H} \left(\boldsymbol{t}_{n} \right) \right|^{2} \\ &= 2 \operatorname{Re} \left\{ e^{j \frac{2\pi}{\lambda} \boldsymbol{t}_{n}^{T} \boldsymbol{a}_{m,j}} \tau_{n,m,j}^{*} \right\} + \left| \tau_{n,m,j} \right|^{2} + 1 \\ &= 2 \left| \tau_{n,m,j} \right| \cos \left(\frac{2\pi}{\lambda} \boldsymbol{t}_{n}^{T} \boldsymbol{a}_{m,j} - \angle \tau_{n,m,j} \right) + \left| \tau_{n,m,j} \right|^{2} + 1, (14) \end{split}$$

with $\tau_{n,m,j} = \sum_{i=1,i\neq n}^{N} e^{j\frac{2\pi}{\lambda}} t_i^T(a_m - a_j)$. Based on (13) and (14), the ergodic rate of the m-th user is given by (15) at the top of this page, where parameters $c_{1,m,j}, c_{2,m}$, and $c_{3,m}$ are respectively defined as

$$c_{1,m,j} = \frac{\beta_j \kappa_m \kappa_j}{(\kappa_m + 1)(\kappa_j + 1)},\tag{16a}$$

$$c_{2,m} = \beta_m \left(\frac{2N\kappa_m + N}{\left(\kappa_m + 1\right)^2} + N^2 \right),\tag{16b}$$

$$c_{3,m} = \sum_{j=1, j \neq m}^{M} c_{1,m,j} \left(|\tau_{n,m,j}|^2 + 1 \right) + \frac{\sigma_m^2 N}{\beta_m P_{\text{tot}}} \sum_{j=1}^{M} \beta_j + \sum_{j=1, j \neq m}^{M} \frac{N \beta_j \left(\kappa_m + \kappa_j + 1 \right)}{\left(\kappa_m + 1 \right) \left(\kappa_j + 1 \right)}.$$
 (16c)

The antenna position optimization problem for t_n with MRT beamforming can now be reformulated as

(P2.n):
$$\max_{\boldsymbol{t}_n} \sum_{m=1}^{M} R_{\text{MRT},m}^{app}(\boldsymbol{t}_n)$$
 (17)
s.t. (6c), (6d).

Although the objective function has been simplified, the term $2\sum_{j=1,j\neq m}^{M}c_{1,m,j}\left|\tau_{n,m,j}\right|\cos\left(\frac{2\pi}{\lambda}\boldsymbol{t}_{n}^{T}\boldsymbol{a}_{m,j}-\angle\tau_{n,m,j}\right)$ in (15), along with its inverse, remains neither concave nor convex with respect to \boldsymbol{t}_{n} . This non-convexity poses a challenge, preventing the construction of a global lower bound for the objective function using the first-order Taylor expansion.

C. Constructing a Surrogate Function via SCA Technique

To address the non-convexity of the objective function in (17), we propose constructing a concave lower-bound surrogate function for t_n by sequentially applying first-order and second-order Taylor expansions.

First, we define the function $b_m(t_n)$, representing the nonconvex term in the denominator of (15)

$$b_{m}(\boldsymbol{t}_{n}) = 2 \sum_{1}^{M} c_{1,m,j} \left| \tau_{n,m,j} \right| \cos \left(\frac{2\pi}{\lambda} \boldsymbol{t}_{n}^{T} \boldsymbol{a}_{m,j} - \angle \tau_{n,m,j} \right).$$
(18)

The expression $R_{\text{MRT},m}^{app}(t_n) = \log_2\left(1 + \frac{c_{2,m}}{b_m(t_n) + c_{3,m}}\right)$ is convex with respect to $b_m(t_n)$. Using the first-order Taylor expansion [34], we derive the following concave lower bound

$$\log_{2}\left(1 + \frac{c_{2,m}}{b_{m}\left(\boldsymbol{t}_{n}\right) + c_{3,m}}\right) \geq \log_{2}\left(1 + \frac{c_{2,m}}{b_{m}\left(\boldsymbol{t}_{n}^{\ell}\right) + c_{3,m}}\right)$$
$$-\frac{c_{2,m}\log_{2}e}{\left(b_{m}\left(\boldsymbol{t}_{n}^{\ell}\right) + c_{3,m}\right)\left(b_{m}\left(\boldsymbol{t}_{n}^{\ell}\right) + c_{2,m} + c_{3,m}\right)}$$
$$\times\left(b_{m}\left(\boldsymbol{t}_{n}\right) - b_{m}\left(\boldsymbol{t}_{n}^{\ell}\right)\right),\tag{19}$$

where \boldsymbol{t}_n^{ℓ} represents the local point at the ℓ -th iteration in the SCA process. Nevertheless, $b_m(\boldsymbol{t}_n^{\ell})$ is still neither concave nor convex with respect to \boldsymbol{t}_n , requiring further refinement to achieve a more tractable optimization framework.

To overcome this challenge, we apply the second-order Taylor expansion (also known as the Descent Lemma [35, Lemma 12]) to construct a convex upper-bound surrogate function for $b_m(\boldsymbol{t}_n^\ell)$. Specifically, we introduce a positive scalar $\psi_{m,n}$ such that $\psi_{m,n}\boldsymbol{I} \succeq \nabla^2 b_m(\boldsymbol{t}_n)$. This ensures the following inequality

$$b_{m}\left(\boldsymbol{t}_{n}\right) \leq b_{m}\left(\boldsymbol{t}_{n}^{\ell}\right) + \nabla b_{m}\left(\boldsymbol{t}_{n}^{\ell}\right)^{T}\left(\boldsymbol{t}_{n} - \boldsymbol{t}_{n}^{\ell}\right)$$
$$+ \frac{\psi_{m,n}}{2}\left(\boldsymbol{t}_{n} - \boldsymbol{t}_{n}^{\ell}\right)^{T}\left(\boldsymbol{t}_{n} - \boldsymbol{t}_{n}^{\ell}\right)$$
$$\triangleq g_{m}^{\text{ub},\ell}\left(\boldsymbol{t}_{n}\right), \tag{20}$$

$$\frac{\partial b_m\left(\boldsymbol{t}_n\right)}{\partial x_n}\Big|_{\boldsymbol{t}_n=\boldsymbol{t}_n^{\ell}} = -\frac{4\pi}{\lambda} \sum_{j=1, j \neq m}^{M} c_{1,m,j} \left| \tau_{n,m,j} \right| \left(\cos \theta_m \sin \phi_m - \cos \theta_j \sin \phi_j\right) \sin \left(\frac{2\pi}{\lambda} \boldsymbol{t}_n^T \left(\boldsymbol{a}_m - \boldsymbol{a}_j\right) - \angle \tau_{n,m,j}\right), \quad (22a)$$

$$\frac{\partial b_m\left(\boldsymbol{t}_n\right)}{\partial y_n}\Big|_{\boldsymbol{t}_n=\boldsymbol{t}_n^{\ell}} = -\frac{4\pi}{\lambda} \sum_{j=1, j \neq m}^{M} c_{1,m,j} \left| \tau_{n,m,j} \right| \left(\sin \theta_m - \sin \theta_j \right) \sin \left(\frac{2\pi}{\lambda} \boldsymbol{t}_n^T \left(\boldsymbol{a}_m - \boldsymbol{a}_j \right) - \angle \tau_{n,m,j} \right). \tag{22b}$$

$$\frac{\partial b_{m}(\boldsymbol{t}_{n})}{\partial x_{n}\partial x_{n}} = -\frac{8\pi^{2}}{\lambda^{2}} \sum_{j=1, j\neq m}^{M} c_{1,m,j} \left| \tau_{n,m,j} \right| \left(\cos \theta_{m} \sin \phi_{m} - \cos \theta_{j} \sin \phi_{j} \right)^{2} \cos \left(\frac{2\pi}{\lambda} \boldsymbol{t}_{n}^{T} \left(\boldsymbol{a}_{m} - \boldsymbol{a}_{j} \right) - \angle \tau_{n,m,j} \right), \tag{24a}$$

$$\frac{\partial b_{m}(\boldsymbol{t}_{n})}{\partial x_{n}\partial y_{n}} = \frac{\partial b_{m}(\boldsymbol{t}_{n})}{\partial y_{n}\partial x_{n}}$$

$$= -\frac{8\pi^{2}}{\lambda^{2}} \sum_{j=1, j\neq m}^{M} c_{1,m,j} \left| \tau_{n,m,j} \right| \left(\cos \theta_{m} \sin \phi_{m} - \cos \theta_{j} \sin \phi_{j} \right) \left(\sin \theta_{m} - \sin \theta_{j} \right) \cos \left(\frac{2\pi}{\lambda} \boldsymbol{t}_{n}^{T} \left(\boldsymbol{a}_{m} - \boldsymbol{a}_{j} \right) - \angle \tau_{n,m,j} \right), \tag{24b}$$

$$\frac{\partial b_{m}(\boldsymbol{t}_{n})}{\partial y_{n}\partial y_{n}} = -\frac{8\pi^{2}}{\lambda^{2}} \sum_{j=1, j\neq m}^{M} c_{1,m,j} \left| \tau_{n,m,j} \right| \left(\sin \theta_{m} - \sin \theta_{j} \right)^{2} \cos \left(\frac{2\pi}{\lambda} \boldsymbol{t}_{n}^{T} \left(\boldsymbol{a}_{m} - \boldsymbol{a}_{j} \right) - \angle \tau_{n,m,j} \right). \tag{24c}$$

where the gradient $\nabla b_m\left(\boldsymbol{t}_n^{\ell}\right)$ is computed as

$$\nabla b_m \left(\boldsymbol{t}_n^{\ell} \right) = \left[\frac{\partial b_m \left(\boldsymbol{t}_n \right)}{\partial x_n} \Big|_{\boldsymbol{t}_n = \boldsymbol{t}_n^{\ell}}, \frac{\partial b_m \left(\boldsymbol{t}_n \right)}{\partial y_n} \Big|_{\boldsymbol{t}_n = \boldsymbol{t}_n^{\ell}} \right], \quad (21)$$

with the detailed expressions of $\frac{\partial b_m(t_n)}{\partial x_n}$ $|_{t_n=t_n^\ell}$ and $\frac{\partial b_m(t_n)}{\partial y_n}$ $|_{t_n=t_n^\ell}$ provided in (22) at the top of this page. Next, we determine the scalar $\psi_{m,n}$ such that it meets the constraint $\psi_{m,n} I \succeq \nabla^2 b_m(t_n)$, ensuring a suitable upperbound approximation. To start with, we calculate the Hessian matrix $\nabla^2 b_m(t_n)$, which is expressed as

$$\nabla^{2}b_{m}\left(\boldsymbol{t}_{n}\right) = \begin{bmatrix} \frac{\partial b_{m}\left(\boldsymbol{t}_{n}\right)}{\partial x_{n}\partial x_{n}} & \frac{\partial b_{m}\left(\boldsymbol{t}_{n}\right)}{\partial x_{n}\partial y_{n}} \\ \frac{\partial b_{m}\left(\boldsymbol{t}_{n}\right)}{\partial y_{n}\partial x_{n}} & \frac{\partial b_{m}\left(\boldsymbol{t}_{n}\right)}{\partial y_{n}\partial y_{n}} \end{bmatrix}, \tag{23}$$

with the detailed entries of this matrix provided in (24) at the top of this page. The basic scaling concept, as presented in [15] and [23], is expressed as

$$\|\nabla^{2}b_{m}(\boldsymbol{t}_{n})\|_{2} \leq \|\nabla^{2}b_{m}(\boldsymbol{t}_{n})\|_{F}$$

$$\leq \|\Psi_{11} \quad \Psi_{12}\|_{F} \triangleq \bar{\psi}_{m,n}, \qquad (25)$$

where the matrix $\Psi = \begin{bmatrix} \Psi_{11} & \Psi_{12} \\ \Psi_{12} & \Psi_{22} \end{bmatrix}$ in (26) has entries defined as

$$\Psi_{11} = \sum_{j=1, j \neq m}^{M} c_{1,m,j} \left| \tau_{n,m,j} \right| \left(\cos \theta_m \sin \phi_m - \cos \theta_j \sin \phi_j \right)^2,$$

$$\Psi_{12} = \sum_{j=1, j \neq m}^{M} c_{1,m,j} \left| \tau_{n,m,j} \right| \left| (\cos \theta_m \sin \phi_m - \cos \theta_j \sin \phi_j) \right| \times (\sin \theta_m - \sin \theta_i) \right|, \tag{26b}$$

$$\Psi_{22} = \sum_{j=1, j \neq m}^{M} c_{1,m,j} \left| \tau_{n,m,j} \right| \left(\sin \theta_{m} - \sin \theta_{j} \right)^{2}, \tag{26c}$$

by simplifying $\cos\left(\frac{2\pi}{\lambda}\boldsymbol{t}_n^T\boldsymbol{a}_{m,j}-\angle\boldsymbol{\tau}_{n,m,j}\right)=1, \forall j\neq m,$ and taking absolute values for $\left(\cos\theta_m\sin\phi_m-\cos\theta_j\sin\phi_j\right)\times\left(\sin\theta_m-\sin\theta_j\right), \forall j\neq m, \ \frac{\partial b_m(\boldsymbol{t}_n)}{\partial x_n\partial x_n}, \frac{\partial b_m(\boldsymbol{t}_n)}{\partial x_n\partial y_n}, \ \text{and} \ \frac{\partial b_m(\boldsymbol{t}_n)}{\partial y_n\partial y_n}.$

In fact, the upper bound in (20), influenced by $\psi_{m,n}$, can be further tightened by selecting $\psi_{m,n}$ as follows

$$\|\nabla^{2}b_{m}\left(\boldsymbol{t}_{n}\right)\|_{2} \leq \left\|\begin{vmatrix}\frac{\partial b_{m}\left(\boldsymbol{t}_{n}\right)}{\partial x_{n}\partial x_{n}} & \frac{\partial b_{m}\left(\boldsymbol{t}_{n}\right)}{\partial x_{n}\partial y_{n}} \\ \frac{\partial b_{m}\left(\boldsymbol{t}_{n}\right)}{\partial y_{n}\partial x_{n}} & \frac{\partial b_{m}\left(\boldsymbol{t}_{n}\right)}{\partial y_{n}\partial y_{n}}\end{vmatrix}\right\|_{2}$$

$$\leq \left\|\frac{\Psi_{11}}{\Psi_{12}} \frac{\Psi_{12}}{\Psi_{22}}\right\|_{2} \triangleq \psi_{m,n}, \tag{27}$$

still ensuring that $\psi_{m,n} \mathbf{I} \succeq \nabla^2 b_m(\mathbf{t}_n)$. Compared to $\bar{\psi}_{m,n}$ in (25), the refined bound satisfies

$$\psi_{m,n} \triangleq \begin{vmatrix} |\Psi_{11} & \Psi_{12}| \\ |\Psi_{12} & \Psi_{22}| \\ |\Psi_{12} & \Psi_{22}| \end{vmatrix}_2 \le \begin{vmatrix} |\Psi_{11} & \Psi_{12}| \\ |\Psi_{12} & \Psi_{22}| \\ |F| & = \bar{\psi}_{m,n}.$$
 (28)

The refined bound $\psi_{m,n}$ provides a more accurate upper bound for the surrogate function used in the optimization process. Using the matrix 2-norm and eigenvalue formulas, $\psi_{m,n}$ can be readily computed as

$$\psi_{m,n} = \frac{8\pi^2}{\lambda^2} \epsilon_{\text{max}} (\boldsymbol{\Psi})$$

$$= \frac{4\pi^2}{\lambda^2} \left(\Psi_{11} + \Psi_{22} + \sqrt{(\Psi_{11} - \Psi_{22})^2 - 4\Psi_{12}^2} \right),$$
 (29a)

where $\epsilon_{\max}(\cdot)$ denotes the maximum eigenvalue of a matrix.

With the above transformation, we construct a convex upper-bound surrogate function for $b_m(t_n^\ell)$ and, consequently, derive a concave lower-bound surrogate function for (18). This approach, combined with the first-order approximation in (19), facilitates the design of an efficient antenna position optimization algorithm that iteratively refines the solution within the SCA framework. The sole remaining hurdle in solving the problem (P2.n) lies in the non-convex minimum distance constraint (6d), which is equivalent to ensuring that $\geq D_{\min}^2, \forall n, i \in \mathcal{N}, i \neq n$. Given that $\|t_n - t_i\|^2$ is convex with respect to t_n , it is lower bounded by its first-order Taylor expansion as follows

$$\|\boldsymbol{t}_{n} - \boldsymbol{t}_{i}\|^{2} \geq \|\boldsymbol{t}_{n}^{\ell} - \boldsymbol{t}_{i}\|^{2} + 2\left(\boldsymbol{t}_{n}^{\ell} - \boldsymbol{t}_{i}\right)^{T}\left(\boldsymbol{t}_{n} - \boldsymbol{t}_{n}^{\ell}\right)$$

$$\stackrel{\triangle}{=} \mathcal{T}^{\text{lb},\ell}\left(\boldsymbol{t}_{n}\right). \tag{30}$$

Algorithm 1 AO-based optimization algorithm for (P2).

- 1: **Initialize:** Set initial antenna positions t_n^0 and initialize the iteration counter $\ell = 0$.
- 2: repeat
- Compute the required parameters for the surrogate 3: function in (31a), including $\psi_{m,n}$ derived in (29).
- For each iteration, solve the problem (P3.n) for Nantennas using convex optimization methods obtain updated antenna positions $t_n^{\ell+1}$.
- Set $\ell = \ell + 1$.
- 6: until The fractional increase of (31a) between two consecutive iterations is below a threshold ζ .

D. Overall Algorithm and Computational Complexity Analysis

By substituting the objective function with the surrogate function that combines (18) and (19) and replacing $||t_n - t_i||^2$ with $\mathcal{T}^{\text{lb},\ell}\left(t_{n}\right)$, the approximation optimization problem is

$$(P3.n): \max_{\boldsymbol{t}_{n}} \sum_{m=1}^{M} \log_{2} \left(1 + \frac{c_{2,m}}{b_{m} \left(\boldsymbol{t}_{n}^{\ell} \right) + c_{3,m}} \right) \\ - \frac{c_{2,m} \log_{2} e}{\left(b_{m} \left(\boldsymbol{t}_{n}^{\ell} \right) + c_{3,m} \right) \left(b_{m} \left(\boldsymbol{t}_{n}^{\ell} \right) + c_{3,m} + c_{2,m} \right)} \\ \times \left(\nabla b_{m} \left(\boldsymbol{t}_{n}^{\ell} \right)^{T} \left(\boldsymbol{t}_{n} - \boldsymbol{t}_{n}^{\ell} \right) + \frac{\psi_{m,n}}{2} \| \boldsymbol{t}_{n} - \boldsymbol{t}_{n}^{\ell} \|^{2} \right) (31a) \\ \text{s.t. } \mathcal{T}^{\text{lb},\ell}(\boldsymbol{t}_{n}) \geq D_{\min}^{2}, \forall n, i \in \mathcal{N}, \tag{31b} \\ (6d).$$

As a convex QCP, this problem can be solved efficiently using standard solvers such as CVX [36]. By solving (P3.n), we obtain a lower bound on the optimal value of (P2.n).

The overall AO-based algorithm is detailed in Algorithm 1, deriving a solution for the problem (P2) by iteratively solving (P3.n). The algorithm guarantees convergence to local optimal points since the objective value is non-decreasing in each iteration. Given that the problem is a QCP, the overall computational complexity of Algorithm 1 is $\mathcal{O}(L_1 \ln \frac{1}{\varepsilon} N^{4.5})$ [37], where L_1 represents the number of iterations required for convergence, and ε denotes the prescribed accuracy.

IV. ACHIEVABLE RATE DERIVATION AND ANTENNA POSITION OPTIMIZATION UNDER ZF BEAMFORMING

In this section, we extend our analysis and design to the case with ZF beamforming. We first derive a lower bound on the ergodic rate under equal power allocation, leveraging statistical CSI and the structure of small-timescale ZF beamforming. These expressions are then utilized for MAs' position optimization in an antenna-wise manner, enhancing large-timescale performance.

A. Ergodic Rate Analysis with ZF beamforming

With ZF beamforming, multiuser interference is completely eliminated. Following the approach in [33, Theorem 4], the ZF transmit beamforming vector for user m is expressed as

$$w_{\text{ZF},m} = \sqrt{p_m}$$

$$\times \frac{(\boldsymbol{I}_N - \boldsymbol{B}_n(\boldsymbol{t}) (\boldsymbol{B}_m^H(\boldsymbol{t}) \boldsymbol{B}_n(\boldsymbol{t}))^{-1} \boldsymbol{B}_m^H(\boldsymbol{t})) \boldsymbol{h}_m(\boldsymbol{t})}{\|(\boldsymbol{I}_N - \boldsymbol{B}_n(\boldsymbol{t}) (\boldsymbol{B}_m^H(\boldsymbol{t}) \boldsymbol{B}_n(\boldsymbol{t}))^{-1} \boldsymbol{B}_m^H(\boldsymbol{t})) \boldsymbol{h}_m(\boldsymbol{t})\|}, (32)$$

where p_m represents the power equally allocated to user m, and $B_n(t)$ is defined as the projection matrix for user m's channel, ensuring orthogonality to other users' channels

$$B_{n}(t) = [h_{1}(t), \dots, h_{m-1}(t), h_{m+1}(t), \dots, h_{M}(t)].$$
 (33)

Substituting (33) into (4) and applying equal power allocation

$$p_m = p = \frac{P_{\text{tot}}}{M},\tag{34}$$

the resulting SNR at the receiver for user m is given by

$$\gamma_{\mathrm{ZF},m} = \frac{p_m}{\sigma_m^2}$$

$$\times \frac{|\boldsymbol{h}_{m}^{H}(t)(\boldsymbol{I}_{N}-\boldsymbol{B}_{n}(t)(\boldsymbol{B}_{m}^{H}(t)\boldsymbol{B}_{n}(t))^{-1}\boldsymbol{B}_{m}^{H}(t))\boldsymbol{h}_{m}(t)|^{2}}{\|(\boldsymbol{I}_{N}-\boldsymbol{B}_{n}(t)(\boldsymbol{B}_{m}^{H}(t)\boldsymbol{B}_{n}(t))^{-1}\boldsymbol{B}_{m}^{H}(t))\boldsymbol{h}_{m}(t)\|^{2}}$$

$$=\frac{p_{m}}{\sigma_{m}^{2}}\frac{1}{\left[(\boldsymbol{H}^{H}(t)\boldsymbol{H}(t))^{-1}\right]_{mm}},$$
(35)

with $\boldsymbol{H}(t) = [\boldsymbol{h}_1(t), \boldsymbol{h}_2(t), \dots, \boldsymbol{h}_M(t)]$ represents the channel matrix.

With ZF beamforming, the antenna position optimization problem for ergodic sum rate maximization can be recast as

(P4):
$$\max_{\{t_n\}} \mathbb{E}[\log_2(1 + \gamma_{\text{ZF},m})]$$
 (36)
s.t. (6c), (6d).

The exact expression for the ergodic rate under ZF beamforming is challenging to handle. To address this, we employ Jensen's inequality to derive a tight lower-bound approximation [33], which is expressed as

$$\mathbb{E}\left\{\log_{2}\left(1 + \gamma_{\mathsf{ZF},m}\right)\right\} \ge \log_{2}\left(1 + \frac{p_{m}}{\sigma_{m}^{2}} \frac{\beta_{m}\left(N - M\right)}{\left[\boldsymbol{\Sigma}^{-1}\left(\boldsymbol{t}\right)\right]_{mm}}\right)$$

$$\triangleq \mathcal{R}_{\mathsf{ZF},m}^{lb}(\boldsymbol{t}), \tag{37}$$

where the expectation term is calculated based on statistical

CSI, and
$$\Sigma(t)$$
 is defined as
$$\Sigma(t) = \Lambda_1 + \frac{1}{N} \Lambda_2 \bar{\boldsymbol{H}}^H(t) \bar{\boldsymbol{H}}(t) \Lambda_2, \quad (38)$$

with the following deterministic terms and parameters

$$\bar{\boldsymbol{H}}\left(\boldsymbol{t}\right)\triangleq\left[\bar{\boldsymbol{h}}_{1}\left(\boldsymbol{t}\right),\bar{\boldsymbol{h}}_{2}\left(\boldsymbol{t}\right),\ldots,\bar{\boldsymbol{h}}_{M}\left(\boldsymbol{t}\right)\right],$$
 (39a)

$$\boldsymbol{\Lambda}_1 \triangleq (\boldsymbol{\Omega} + \boldsymbol{I}_M)^{-1}, \tag{39b}$$

$$\boldsymbol{\Lambda}_2 \triangleq \left[\boldsymbol{\Omega}\boldsymbol{\Lambda}_1\right]^{\frac{1}{2}},\tag{39c}$$

$$\Omega \triangleq \operatorname{diag}([\kappa_1, \kappa_2, \dots, \kappa_M]).$$
 (39d)

Remark 2: From (37), (38), and (39), we can draw three key insights. First, under ZF beamforming in the two-timescale design, adjusting antenna positions does not enhance the ergodic rate when M=1. This is because $\Sigma(t)$ simplifies to a fixed scalar and $\mathcal{R}^{lb}_{\mathsf{ZF},m}$ becomes a constant in this scenario. Second, if the deterministic LoS component for user m is absent, i.e., $\kappa_m = 0$, MAs cannot effectively reshape the channel, since $\left[\boldsymbol{\Sigma}^{-1}\left(t\right)\right]_{mm}$ in (37) becomes a fixed value of 1. Third, as N becomes very large, the performance gain from MAs diminishes due to the channel hardening effect. In this case, an FPA system without antenna position tuning already achieves asymptotically orthogonal channels for different users, i.e., $\left|\frac{1}{N}\bar{\boldsymbol{H}}_{j}\left(\boldsymbol{t}_{\text{FPA}}\right)\bar{\boldsymbol{H}}_{m}^{H}\left(\boldsymbol{t}_{\text{FPA}}\right)\right|^{2} \rightarrow \boldsymbol{I}_{N}, \forall j,m.$ Consequently, the properties of the ergodic rate in these scenarios are consistent with those described in Remark 1 for MRT beamforming.

$$\boldsymbol{\Theta}_{1,n} = \begin{bmatrix} N - 1 & \sum_{j=1, j \neq n}^{N} e^{j\frac{2\pi}{\lambda} \boldsymbol{t}_{j}^{T}(\boldsymbol{a}_{1} - \boldsymbol{a}_{1})} & \cdots & \sum_{j=1, j \neq n}^{N} e^{j\frac{2\pi}{\lambda} \boldsymbol{t}_{j}^{T}(\boldsymbol{a}_{M} - \boldsymbol{a}_{1})} \\ \sum_{j=1, j \neq n}^{N} e^{j\frac{2\pi}{\lambda} \boldsymbol{t}_{j}^{T}(\boldsymbol{a}_{1} - \boldsymbol{a}_{2})} & N - 1 & \cdots & \sum_{j=1, j \neq n}^{N} e^{j\frac{2\pi}{\lambda} \boldsymbol{t}_{j}^{T}(\boldsymbol{a}_{M} - \boldsymbol{a}_{2})} \\ \vdots & \vdots & \ddots & \vdots \\ \sum_{j=1, j \neq n}^{N} e^{j\frac{2\pi}{\lambda} \boldsymbol{t}_{j}^{T}(\boldsymbol{a}_{1} - \boldsymbol{a}_{M})} & \sum_{j=1, j \neq n}^{N} e^{j\frac{2\pi}{\lambda} \boldsymbol{t}_{j}^{T}(\boldsymbol{a}_{2} - \boldsymbol{a}_{M})} & \cdots & N - 1 \end{bmatrix}$$
 (42)

B. Antenna Position Optimization Based on AO Method

Despite having closed-form expressions for the ergodic rate in (37), the antenna positions remain intricately coupled in the implicit function $[\boldsymbol{\Sigma}^{-1}(t)]_{mm}$, which depends primarily on the LoS components. To tackle this complexity, we propose an element-wise antenna position optimization framework that leverages Woodbury's identity, the MM, and the SCA method.

In this framework, we first derive a tractable expression for the achievable rate concerning the n-th antenna while keeping the positions of the other antennas fixed. Specifically, for the n-th antenna, we can express the effective channel matrix as

$$\bar{\boldsymbol{H}}^{H}\left(\boldsymbol{t}_{n}\right)\bar{\boldsymbol{H}}\left(\boldsymbol{t}_{n}\right)=\bar{\boldsymbol{g}}_{n}\left(\boldsymbol{t}_{n}\right)\bar{\boldsymbol{g}}_{n}^{H}\left(\boldsymbol{t}_{n}\right)+\boldsymbol{\Theta}_{1,n},\qquad(40)$$

where $\bar{q}_n(t_n)$ is defined as the *n*-th row of \bar{H} . i.e.

$$\bar{\boldsymbol{g}}_{n}\left(\boldsymbol{t}_{n}\right) \triangleq \left[e^{j\frac{2\pi}{\lambda}\boldsymbol{t}_{n}^{T}\boldsymbol{a}_{1}}, e^{j\frac{2\pi}{\lambda}\boldsymbol{t}_{n}^{T}\boldsymbol{a}_{2}}, \dots, e^{j\frac{2\pi}{\lambda}\boldsymbol{t}_{n}^{T}\boldsymbol{a}_{M}}\right]^{H} \in \mathbb{C}^{M \times 1}, (41)$$

and the matrix $\Theta_{1,n}$ is provided in (42) at the top of this page. Using these definitions, the matrix $\Sigma(t_n)$ is expressed as

$$\Sigma(t_n) = \Theta_{2,n} + \frac{1}{N} \Lambda_2 \bar{g}_n(t_n) \bar{g}_n^H(t_n) \Lambda_2, \quad (43)$$

with $\Theta_{2,n} \triangleq \Lambda_1 + \frac{1}{N} \Lambda_2 \Theta_{1,n} \Lambda_2$. Given that $\Lambda_1 \succ 0$, $\Theta_{2,n} \succ 0$, $\Theta_{2,n}^{-1} \succ 0$, and $\Theta_{2,n}^H$ is Hermitian, we can apply Woodbury's identity to rewrite $\Sigma^{-1}(t_n)$ as follows [38]

$$\Sigma^{-1}(\boldsymbol{t}_{n}) = \left(\boldsymbol{\Theta}_{2,n} + \boldsymbol{\Lambda}_{2}\bar{\boldsymbol{g}}_{n}(\boldsymbol{t}_{n})\frac{1}{N}\bar{\boldsymbol{g}}_{n}^{H}(\boldsymbol{t}_{n})\boldsymbol{\Lambda}_{2}\right)^{-1}$$
(44a)
$$= \boldsymbol{\Theta}_{2,n}^{-1} - \frac{\boldsymbol{\Theta}_{2,n}^{-1}\boldsymbol{\Lambda}_{2}\bar{\boldsymbol{g}}_{n}(\boldsymbol{t}_{n})\bar{\boldsymbol{g}}_{n}^{H}(\boldsymbol{t}_{n})\boldsymbol{\Lambda}_{2}\boldsymbol{\Theta}_{2,n}^{-1}}{N + \bar{\boldsymbol{g}}_{n}^{H}(\boldsymbol{t}_{n})\boldsymbol{\Lambda}_{2}\boldsymbol{\Theta}_{2,n}^{-1}\boldsymbol{\Lambda}_{2}\bar{\boldsymbol{g}}_{n}(\boldsymbol{t}_{n})}.$$
(44b)

Remark 3: From (44b), we derive the following inequality

$$[\Sigma^{-1}(t_n)]_{mm} \le [\Theta_{2,n}^{-1}]_{mm} = [\Sigma^{-1}(t_{\text{FPA},n})]_{mm}.$$
 (45)

The inequality holds strictly with MAs, whereas equality is achieved in the FPA case for the n-th antenna. This observation demonstrates that MAs offer a performance gain over FPAs by reducing the inverse channel matrix component $[\boldsymbol{\varSigma}^{-1}\left(t_{n}
ight)]_{mm}$. Specifically, this reduction indicates a decrease in channel correlation between user m and other users while maintaining the channel power gain for user m.

Then, $[\boldsymbol{\Sigma}^{-1}(t_n)]_{mm}$ can be expressed more compactly as

$$\begin{split} & \left[\boldsymbol{\mathcal{E}}^{-1} \left(\boldsymbol{t}_{n} \right) \right]_{mm} \\ & = \left[\boldsymbol{\mathcal{O}}_{2,n}^{-1} \right]_{mm} - \frac{ \left[\boldsymbol{\mathcal{O}}_{2,n}^{-1} \boldsymbol{\Lambda}_{2} \bar{\boldsymbol{g}}_{n} \left(\boldsymbol{t}_{n} \right) \bar{\boldsymbol{g}}_{n}^{H} \left(\boldsymbol{t}_{n} \right) \boldsymbol{\Lambda}_{2} \boldsymbol{\mathcal{O}}_{2,n}^{-1} \right]_{mm} }{ N + \bar{\boldsymbol{g}}_{n}^{H} \left(\boldsymbol{t}_{n} \right) \boldsymbol{\Lambda}_{2} \boldsymbol{\mathcal{O}}_{2,n}^{-1} \boldsymbol{\Lambda}_{2} \bar{\boldsymbol{g}}_{n} \left(\boldsymbol{t}_{n} \right) } \\ & = \frac{ \bar{\boldsymbol{g}}_{n}^{H} \left(\boldsymbol{t}_{n} \right) \left[\boldsymbol{\mathcal{O}}_{2,n}^{-1} \right]_{mm} \boldsymbol{Y}_{n} \bar{\boldsymbol{g}}_{n} \left(\boldsymbol{t}_{n} \right) }{ \bar{\boldsymbol{g}}_{n}^{H} \left(\boldsymbol{t}_{n} \right) \boldsymbol{Y}_{n} \bar{\boldsymbol{g}}_{n} \left(\boldsymbol{t}_{n} \right) } - \frac{ \boldsymbol{l}_{n,m}^{H} \bar{\boldsymbol{g}}_{n} \left(\boldsymbol{t}_{n} \right) \bar{\boldsymbol{g}}_{n}^{H} \left(\boldsymbol{t}_{n} \right) \boldsymbol{l}_{n,m} }{ \bar{\boldsymbol{g}}_{n}^{H} \left(\boldsymbol{t}_{n} \right) \boldsymbol{Y}_{n} \bar{\boldsymbol{g}}_{n} \left(\boldsymbol{t}_{n} \right) } \\ & = \frac{ \bar{\boldsymbol{g}}_{n}^{H} \left(\boldsymbol{t}_{n} \right) \left\{ \left[\boldsymbol{\mathcal{O}}_{2,n}^{-1} \right]_{mm} \boldsymbol{Y}_{n} - \boldsymbol{l}_{n,m} \boldsymbol{l}_{n,m}^{H} \right\} \bar{\boldsymbol{g}}_{n} \left(\boldsymbol{t}_{n} \right) }{ \bar{\boldsymbol{g}}_{n}^{H} \left(\boldsymbol{t}_{n} \right) \boldsymbol{X}_{n,m} \bar{\boldsymbol{g}}_{n} \left(\boldsymbol{t}_{n} \right) } \\ & = \frac{ \bar{\boldsymbol{g}}_{n}^{H} \left(\boldsymbol{t}_{n} \right) \boldsymbol{X}_{n,m} \bar{\boldsymbol{g}}_{n} \left(\boldsymbol{t}_{n} \right) }{ \bar{\boldsymbol{g}}_{n}^{H} \left(\boldsymbol{t}_{n} \right) \boldsymbol{Y}_{n} \bar{\boldsymbol{g}}_{n} \left(\boldsymbol{t}_{n} \right) } . \end{split} \tag{46}$$

where we define the following vectors and matrices

$$\boldsymbol{Y}_{n} = \frac{N}{M} \boldsymbol{I}_{M} + \boldsymbol{\Lambda}_{2} \boldsymbol{\Theta}_{2,n}^{-1} \boldsymbol{\Lambda}_{2}, \tag{47a}$$

$$\boldsymbol{l}_{n,m}^{H} = \left[\boldsymbol{\Theta}_{2,n}^{-1} \boldsymbol{\Lambda}_{2}\right]_{(m,n)} m \tag{47b}$$

$$\boldsymbol{X}_{n,m} = \left[\boldsymbol{\Theta}_{2,n}^{-1}\right]_{mm} \boldsymbol{Y}_n - \boldsymbol{l}_{n,m} \boldsymbol{l}_{n,m}^H, \tag{47c}$$

with $[\cdot]_{(m,:)}$ referred to the m-th row vector of a matrix.

Based on this, the lower bound on the ergodic rate for user m is given by

$$R_{\mathrm{ZF},m}^{\mathrm{lb,1}}(\boldsymbol{t}_{n}) = \log_{2}\left(1 + \eta_{m} \frac{\bar{\boldsymbol{g}}_{n}^{H}(\boldsymbol{t}_{n}) \boldsymbol{Y}_{n} \bar{\boldsymbol{g}}_{n}(\boldsymbol{t}_{n})}{\bar{\boldsymbol{q}}_{n}^{H}(\boldsymbol{t}_{n}) \boldsymbol{X}_{n} m \bar{\boldsymbol{q}}_{n}(\boldsymbol{t}_{n})}\right), \quad (48)$$

where we denote $\eta_m = \frac{p_m}{\sigma_m^2} \beta_m \left(N-M\right)$ for brevity. The antenna position optimization problem for t_n with ZF beamforming can be reformulated as

(P4.n):
$$\max_{\boldsymbol{t}_n} \sum_{m=1}^{M} R_{\text{ZF},m}^{\text{lb},1}(\boldsymbol{t}_n)$$
 (49)
s.t. (6c), (6d).

Although the objective function is simplified, the fractional term $\frac{\bar{g}_n^H(t_n)Y_n\bar{g}_n(t_n)}{\bar{g}_n^H(t_n)X_{n,m}\bar{g}_n(t_n)}$ remains neither concave nor convex with respect to t_n , presenting challenges in constructing a global concave lower bound for the objective function.

C. Constructing a Surrogate Function via MM and SCA

To address the non-convexity of the objective function in (49), we construct a concave lower-bound surrogate function for t_n through a two-step process. This involves applying the MM method followed by the second-order Taylor expansion. The first step is summarized in the following lemma [39].

Lemma 1: $R_{\text{ZF }m}^{\text{lb}}\left(\boldsymbol{t}_{n}\right)$ is lower bounded by

$$R_{\text{ZF},m}^{\text{lb},1}(\boldsymbol{t}_{n}) \leq R_{\text{ZF},m}^{\text{lb},2}(\boldsymbol{t}_{n})$$

$$= \log_{2} \left(1 + \eta_{m} f_{n,m} \left(\bar{\boldsymbol{g}}_{n}\left(\boldsymbol{t}_{n}\right)\right)\right), \qquad (50)$$

where the fractional term $\frac{\bar{g}_n^H(t_n)Y_n\bar{g}_n(t_n)}{\bar{g}_n^H(t_n)X_{n,m}\bar{g}_n(t_n)}$ in (48) is replaced by the function $f_{n,m}\left(\bar{g}_n\left(t_n\right)\right)$, defined as

$$\begin{split} &f_{n,m}\left(\bar{\boldsymbol{g}}_{n}\left(\boldsymbol{t}_{n}\right)\right) \\ &\triangleq \frac{2\operatorname{Re}\left\{\bar{\boldsymbol{g}}_{n}^{H}\left(\boldsymbol{t}_{n}^{\ell}\right)\boldsymbol{Y}_{n}\bar{\boldsymbol{g}}_{n}\left(\boldsymbol{t}_{n}\right)\right\}}{\bar{\boldsymbol{g}}_{n}^{H}\left(\boldsymbol{t}_{n}^{\ell}\right)\boldsymbol{X}_{n,m}\bar{\boldsymbol{g}}_{n}\left(\boldsymbol{t}_{n}^{\ell}\right)} - \frac{\bar{\boldsymbol{g}}_{n}^{H}\left(\boldsymbol{t}_{n}^{\ell}\right)\boldsymbol{Y}_{n}\bar{\boldsymbol{g}}_{n}\left(\boldsymbol{t}_{n}^{\ell}\right)}{\left(\bar{\boldsymbol{g}}_{n}^{H}\left(\boldsymbol{t}_{n}^{\ell}\right)\boldsymbol{X}_{n,m}\bar{\boldsymbol{g}}_{n}\left(\boldsymbol{t}_{n}^{\ell}\right)\right)^{2}} \\ &\times \left\{2\lambda_{\max}\left(\boldsymbol{X}_{n,m}\right)\boldsymbol{M} - \bar{\boldsymbol{g}}_{n}^{H}\left(\boldsymbol{t}_{n}^{\ell}\right)\boldsymbol{X}_{n,m}\bar{\boldsymbol{g}}_{n}\left(\boldsymbol{t}_{n}^{\ell}\right)\right. \\ &\left. + 2\operatorname{Re}\left\{\bar{\boldsymbol{g}}_{n}^{H}\left(\boldsymbol{t}_{n}^{\ell}\right)\left[\boldsymbol{X}_{n,m} - \lambda_{\max}\left(\boldsymbol{X}_{n,m}\right)\boldsymbol{I}_{M}\right]\bar{\boldsymbol{g}}_{n}\left(\boldsymbol{t}_{n}\right)\right\}\right\}. (51) \end{split}$$

Proof: The function $\log (1 + v)$ is a concavity-preserving transformation, so our task is to find a concave lower bound for $\begin{array}{l} \frac{\bar{g}_{n}^{H}(t_{n})Y_{n}\bar{g}_{n}(t_{n})}{\bar{g}_{n}^{H}(t_{n})X_{n,m}\bar{g}_{n}(t_{n})}. \text{ Define } r_{n,m}\left(t_{n}\right) \triangleq \bar{g}_{n}^{H}\left(t_{n}\right)X_{n,m}\bar{g}_{n}\left(t_{n}\right). \\ \text{Since } Y_{n}, \text{ defined in (46a), is positive definite, the function } \\ \frac{\bar{g}_{n}^{H}(t_{n})Y_{n}\bar{g}_{n}(t_{n})}{r_{n,m}(t_{n})} \text{ is jointly convex with respect to } \bar{g}_{n}\left(t_{n}\right) \text{ and } \end{array}$ $r_{n,m}(t_n)$. Due to this convexity, the following inequality can be derived using the first-order Taylor expansion

$$\frac{\bar{g}_{n}^{H}\left(t_{n}\right)Y_{n}\bar{g}_{n}\left(t_{n}\right)}{r_{n,m}\left(t_{n}\right)} \geq \frac{\bar{g}_{n}^{H}\left(t_{n}^{\ell}\right)Y_{n}\bar{g}_{n}\left(t_{n}^{\ell}\right)}{r_{n,m}^{\ell}\left(t_{n}\right)} + \frac{\partial\left(\frac{\bar{g}_{n}^{H}\left(t_{n}\right)Y_{n}\bar{g}_{n}\left(t_{n}\right)}{r_{n,m}\left(t_{n}\right)}\right)}{\partial r_{n,m}\left(t_{n}\right)} \bigg|_{t_{n}=t_{n}^{\ell}} \left(r_{n,m}\left(t_{n}\right) - r_{n,m}\left(t_{n}^{\ell}\right)\right) \\
\left(\frac{\partial\left(\frac{\bar{g}_{n}^{H}\left(t_{n}\right)Y_{n}\bar{g}_{n}\left(t_{n}\right)}{r_{n,m}\left(t_{n}\right)}\right)}{\partial \bar{g}_{n}\left(t_{n}\right)} \bigg|_{t_{n}=t_{n}^{\ell}}\right)^{H} \left(\bar{g}_{n}\left(t_{n}\right) - \bar{g}_{n}\left(t_{n}^{\ell}\right)\right). (52)$$

After calculating (52), the following inequalities can be established as a lower bound

$$\frac{\bar{\mathbf{g}}_{n}^{H}\left(\mathbf{t}_{n}\right)\boldsymbol{Y}_{n}\bar{\mathbf{g}}_{n}\left(\mathbf{t}_{n}\right)}{r_{n,m}\left(\mathbf{t}_{n}\right)} \geq \frac{2\operatorname{Re}\left\{\bar{\mathbf{g}}_{n}^{H}\left(\mathbf{t}_{n}^{\ell}\right)\boldsymbol{Y}_{n}\bar{\mathbf{g}}_{n}\left(\mathbf{t}_{n}\right)\right\}}{\bar{\mathbf{g}}_{n}^{H}\left(\mathbf{t}_{n}^{\ell}\right)\boldsymbol{X}_{n,m}\bar{\mathbf{g}}_{n}\left(\mathbf{t}_{n}^{\ell}\right)} - \frac{\bar{\mathbf{g}}_{n}^{H}\left(\mathbf{t}_{n}^{\ell}\right)\boldsymbol{Y}_{n}\bar{\mathbf{g}}_{n}\left(\mathbf{t}_{n}^{\ell}\right)}{\left(\bar{\mathbf{g}}_{n}^{H}\left(\mathbf{t}_{n}^{\ell}\right)\boldsymbol{X}_{n,m}\bar{\mathbf{g}}_{n}\left(\mathbf{t}_{n}^{\ell}\right)\right)^{2}}\bar{\mathbf{g}}_{n}^{H}\left(\mathbf{t}_{n}\right)\boldsymbol{X}_{n,m}\bar{\mathbf{g}}_{n}\left(\mathbf{t}_{n}\right). (53)$$

Note that the quadratic form in (53) is further bounded by

$$\begin{split} & \bar{\boldsymbol{g}}_{n}^{H}\left(\boldsymbol{t}_{n}\right)\boldsymbol{X}_{n,m}\bar{\boldsymbol{g}}_{n}\left(\boldsymbol{t}_{n}\right) \\ & \leq \bar{\boldsymbol{g}}_{n}^{H}\left(\boldsymbol{t}_{n}\right)\lambda_{\max}\left(\boldsymbol{X}_{n,m}\right)\boldsymbol{I}_{M}\bar{\boldsymbol{g}}\left(\boldsymbol{t}_{n}\right) \\ & + 2\mathrm{Re}\left\{\bar{\boldsymbol{g}}_{n}^{H}\left(\boldsymbol{t}_{n}^{\ell}\right)\left[\boldsymbol{X}_{n,m} - \lambda_{\max}\left(\boldsymbol{X}_{n,m}\right)\boldsymbol{I}_{M}\right]\bar{\boldsymbol{g}}_{n}\left(\boldsymbol{t}_{n}\right)\right\} \\ & + \bar{\boldsymbol{g}}_{n}^{H}\left(\boldsymbol{t}_{n}^{\ell}\right)\left[\lambda_{\max}\left(\boldsymbol{X}_{n,m}\right)\boldsymbol{I}_{M} - \boldsymbol{X}_{n,m}\right]\bar{\boldsymbol{g}}_{n}\left(\boldsymbol{t}_{n}^{\ell}\right) \\ & = 2\lambda_{\max}\left(\boldsymbol{X}_{n,m}\right)M - \bar{\boldsymbol{g}}_{n}^{H}\left(\boldsymbol{t}_{n}^{\ell}\right)\boldsymbol{X}_{n,m}\bar{\boldsymbol{g}}_{n}\left(\boldsymbol{t}_{n}^{\ell}\right) \\ & + 2\mathrm{Re}\left\{\bar{\boldsymbol{g}}_{n}^{H}\left(\boldsymbol{t}_{n}^{\ell}\right)\left[\boldsymbol{X}_{n,m} - \lambda_{\max}\left(\boldsymbol{X}_{n,m}\right)\boldsymbol{I}_{M}\right]\bar{\boldsymbol{g}}_{n}\left(\boldsymbol{t}_{n}\right)\right\}. (54) \end{split}$$

By substituting (53) and (54) into (48), we have (50).

Using Lemma 1, the lower-bound ergodic rate of user m in (51) can be reformulated more concisely as

$$\begin{split} R_{\mathrm{ZF},m}^{\mathrm{lb},2}\left(\boldsymbol{t}_{n}\right) &= \log\left(1 + \eta_{m}\left(\chi_{n,m}^{\ell} + \operatorname{Re}\left\{\boldsymbol{q}_{n,m}^{T}\bar{\boldsymbol{g}}_{n}\left(\boldsymbol{t}_{n}\right)\right\}\right)\right) \\ &= \log\left(1 + \eta_{m}\left(\chi_{n,m}^{\ell} + \sum_{u=1}^{M}\left|q_{n,m,u}^{\ell}\right|\right. \\ &\left. \times \cos\left(\frac{2\pi}{\lambda}\boldsymbol{t}_{n}^{T}\boldsymbol{a}_{u} - \angle q_{n,m,u}^{\ell}\right)\right)\right), \end{split}$$
(55)

where we define the constants specific to the optimization of t_n with the positions of the other antennas fixed as follows

$$\chi_{n,m}^{\ell} \triangleq -\frac{\bar{\boldsymbol{g}}_{n}^{H}\left(\boldsymbol{t}_{n}^{\ell}\right) \boldsymbol{Y}_{n} \bar{\boldsymbol{g}}_{n}\left(\boldsymbol{t}_{n}^{\ell}\right)}{\left(\bar{\boldsymbol{g}}_{n}^{H}\left(\boldsymbol{t}_{n}^{\ell}\right) \boldsymbol{X}_{n,m} \bar{\boldsymbol{g}}_{n}\left(\boldsymbol{t}_{n}^{\ell}\right)\right)^{2}} \left(2\lambda_{\max}\left(\boldsymbol{X}_{n,m}\right) \boldsymbol{M}\right) - \bar{\boldsymbol{g}}_{n}^{H}\left(\boldsymbol{t}_{n}^{\ell}\right) \boldsymbol{X}_{n,m} \bar{\boldsymbol{g}}_{n}\left(\boldsymbol{t}_{n}^{\ell}\right)\right), \quad (56)$$

$$\boldsymbol{q}_{n,m} \triangleq \frac{2}{\bar{\boldsymbol{g}}_{n}^{H}\left(\boldsymbol{t}_{n}^{\ell}\right) \boldsymbol{X}_{n,m} \bar{\boldsymbol{g}}_{n}\left(\boldsymbol{t}_{n}^{\ell}\right)} \bar{\boldsymbol{g}}_{n}^{H}\left(\boldsymbol{t}_{n}^{\ell}\right) \left(\boldsymbol{Y}_{n}\right) - \frac{\bar{\boldsymbol{g}}_{n}^{H}\left(\boldsymbol{t}_{n}^{\ell}\right) \boldsymbol{Y}_{n} \bar{\boldsymbol{g}}_{n}\left(\boldsymbol{t}_{n}^{\ell}\right)}{\bar{\boldsymbol{g}}_{n}^{H}\left(\boldsymbol{t}_{n}^{\ell}\right) \boldsymbol{X}_{n,m} \bar{\boldsymbol{g}}_{n}\left(\boldsymbol{t}_{n}^{\ell}\right)} \left(\boldsymbol{X}_{n,m} - \lambda_{\max}\left(\boldsymbol{X}_{n,m}\right) \boldsymbol{I}_{M}\right). \quad (57)$$

Similar to problem (P2), we continue to address the non-convexity of the term $\cos\left(\frac{2\pi}{\lambda}\boldsymbol{t}_n^T\boldsymbol{a}_m-\angle q_{n,m,u}^\ell\right)$ in (55) using the SCA technique. Given the structural similarity of the expressions, the SCA procedure mirrors the content outlined in Section III-C. Specifically, by defining the non-convex non-concave function in (55) as

$$F_{n,m}(\boldsymbol{t}_n) = \sum_{u=1}^{M} \left| q_{n,m,u}^{\ell} \right| \cos \left(\frac{2\pi}{\lambda} \boldsymbol{t}_n^T \boldsymbol{a}_u - \angle q_{n,m,u}^{\ell} \right), \quad (58)$$

Algorithm 2 AO-based optimization algorithm for (P4).

- 1: **Initialize:** Set initial antenna positions t_n^0 and initialize the iteration counter $\ell = 0$.
- 2: repeat
- 3: Compute the required parameters for the surrogate function in (64), including $\xi_{m,n}$ derived in (62).
- 4: For each iteration, solve the problem (P3.n) for N antennas using convex optimization methods obtain updated antenna positions $t_n^{\ell+1}$.
- 5: Set $\ell = \ell + 1$.
- 6: **until** The fractional increase of (65) between two consecutive iterations is below a threshold ζ .

the ergodic rate of user m in (58) is further lower-bounded by

$$\begin{split} R_{\text{ZF},m}^{\text{lb},2}\left(\boldsymbol{t}_{n}\right) &\leq R_{\text{ZF},m}^{\text{lb},3}\left(\boldsymbol{t}_{n}\right) \\ &= \log_{2}\left(1 + \eta_{m}\left(\chi_{n,m}^{\ell} + F_{n,m}(\boldsymbol{t}_{n}^{\ell}) + \nabla z_{m}(\boldsymbol{t}_{n}^{\ell})^{T}\right. \\ &\left. \times \left(\boldsymbol{t}_{n} - \boldsymbol{t}_{n}^{\ell}\right) - \frac{\psi_{m,n}}{2}\|\boldsymbol{t}_{n} - \boldsymbol{t}_{n}^{\ell}\|^{2}\right)\right), \end{split}$$
(59)

where $\nabla(F_{n,m})$ is the gradient of $F_{n,m}$, as provided in (60) at the top of the following page. This concave lower bound is constructed by applying the second-order Taylor expansion

$$F_{n,m}\left(\boldsymbol{t}_{n}\right) \geq F_{n,m}\left(\boldsymbol{t}_{n}^{\ell}\right) + \nabla F_{n,m}\left(\boldsymbol{t}_{n}^{\ell}\right)^{T}\left(\boldsymbol{t}_{n} - \boldsymbol{t}_{n}^{\ell}\right)$$
$$-\frac{\xi_{m,n}}{2}\left(\boldsymbol{t}_{n} - \boldsymbol{t}_{n}^{\ell}\right)^{T}\left(\boldsymbol{t}_{n} - \boldsymbol{t}_{n}^{\ell}\right)$$
$$\triangleq F_{n,m}^{\mathrm{lb},\ell}\left(\boldsymbol{t}_{n}\right),\tag{61}$$

where $\xi_{m,n}$ is a positive real number $\xi_{m,n}$ such that $\xi_{m,n} I \succeq \nabla^2 F_m(t_n)$ and, similar to (29), can be given by

$$\xi_{m,n} = \frac{4\pi^2}{\lambda^2} \epsilon_{\text{max}} (\mathbf{\Xi})$$

$$= \frac{2\pi^2}{\lambda^2} \left(\Xi_{11} + \Xi_{22} + \sqrt{(\Xi_{11} - \Xi_{22})^2 + 4\Xi_{12}^2} \right), (62b)$$

with $\epsilon_{\rm max}(\cdot)$ denoting the maximum eigenvalue and the terms

$$\Xi_{11} = \sum_{u=1}^{M} |q_{n,m,u}^{\ell}| \cos^{2} \theta_{u} \sin^{2} \phi_{u}, \tag{63a}$$

$$\Xi_{12} = \sum_{u=1}^{M} \left| q_{n,m,u}^{\ell} \right| \left| \cos \theta_u \sin \phi_u \sin \theta_u \right|, \tag{63b}$$

$$\Xi_{22} = \sum_{u=1}^{M} |q_{n,m,u}^{\ell}| \sin^2 \theta_u.$$
 (63c)

D. Overall Algorithm and Computational Complexity Analysis

The convex optimization problem for maximizing the lower bound of the ergodic sum rate can now be reformulated as

(P5.n):
$$\max_{\boldsymbol{t}_n} \sum_{m=1}^{M} R_{\text{ZF},m}^{\text{lb},3}(\boldsymbol{t}_n)$$
 (64)
s.t. (29b), (6d).

As a convex QCP, the optimal solution to this problem can be obtained using standard solvers (e.g., CVX [36]).

The overall AO-based algorithm is detailed in Algorithm 2, which iteratively solves (P5.n) to provide a solution for the problem (P4). The algorithm guarantees convergence to a locally optimal solution, as the objective function value is

$$\nabla F_{n,m}\left(\boldsymbol{t}_{n}^{\ell}\right) = \begin{bmatrix} \frac{\partial F_{n,m}(\boldsymbol{t}_{n})}{\partial x_{n}} \Big|_{\boldsymbol{t}_{n} = \boldsymbol{t}_{n}^{\ell}} \\ \frac{\partial F_{n,m}(\boldsymbol{t}_{n})}{\partial y_{n}} \Big|_{\boldsymbol{t}_{n} = \boldsymbol{t}^{\ell}} \end{bmatrix} = \begin{bmatrix} -\frac{2\pi}{\lambda} \sum_{u=1}^{M} \left| q_{n,m,u}^{\ell} \right| \cos \theta_{u} \sin \phi_{u} \sin \left(\frac{2\pi}{\lambda} \boldsymbol{t}_{n}^{\ell,T} \boldsymbol{a}_{u} - \angle q_{n,m,u}^{\ell}\right) \\ -\frac{2\pi}{\lambda} \sum_{u=1}^{M} \left| q_{n,m,u}^{\ell} \right| \sin \theta_{u} \sin \left(\frac{2\pi}{\lambda} \boldsymbol{t}_{n}^{\ell,T} \boldsymbol{a}_{u} - \angle q_{n,m,u}^{\ell}\right) \end{bmatrix}.$$
(60)

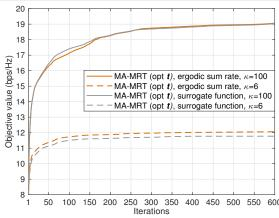


Fig. 3. The convergence of the proposed MA-MRT Algorithm 1. non-decreasing in each iteration. Since the problem is a convex QCP, the overall computational complexity of Algorithm 2 is $\mathcal{O}(L_2 \ln \frac{1}{\varepsilon} N^{4.5})$, where L_2 represents the number of iterations until convergence, and ε denotes the prescribed accuracy.

V. SIMULATION RESULTS

This section provides numerical results to validate the effectiveness of the proposed two-timescale MA-enabled transmission design and our theoretical findings. In the simulations, users are randomly distributed around the BS, with their distances d_m (in meters) uniformly sampled in the range of [50, 70]. The Rician fading channel model is employed with a common Rician factor $\kappa_m = \kappa, \forall m$ for all BS-user channels, providing consistent LoS conditions across users. The large-scale fading factor for each user β_m is modeled as $\beta_m = \beta_0 d_m^{-\alpha}$, where $\beta_0 = -40 \text{dB}$ represents the reference average channel power gain at 1m, and $\alpha = 2.8$ denotes the path-loss exponent. Based on the user distribution, the elevation and azimuth angles of AoD and AoA for each channel path are uniformly distributed within $\left[-\frac{\pi}{2}, \frac{\pi}{2}\right]$. The movable regions for the transmit MAs are set as $\mathcal{C} = \left[-\frac{2}{3}\frac{N_rA\lambda}{2}, \frac{N_rA\lambda}{2}\right] \times \left[-\frac{N_cA\lambda}{2}, \frac{N_cA\lambda}{2}\right]$, which expand adaptively with the number of antennas. Additionally, the minimum antenna spacing is constrained by $D_{\min} = \frac{\lambda}{2}$, and the noise power is fixed at $\sigma_m^2 = -80 \text{dBm}$. The primary antenna-user configuration considered is N=6, M=5, with Rician factors $\kappa=6$ or $\kappa = 100$, representing moderate and strong LoS conditions, respectively. The maximum transmit power P_{tot} is set to 1W, and the region size parameter A is set to 2 unless otherwise stated. Further simulation-specific parameters are outlined in the results section.

In the following, we evaluate the performance of the proposed schemes and compare them to the following benchmarks

- MA with ZF beamforming: Denoted as "MA-ZF (opt t)", this scheme uses ZF beamforming with fixed power allocation (35), and the antenna positions are optimized using Algorithm 2, leveraging two-timescale CSI.
- MA with MRT beamforming: Denoted by "MA-MRT (opt t)", this scheme employs simple MRT beamforming

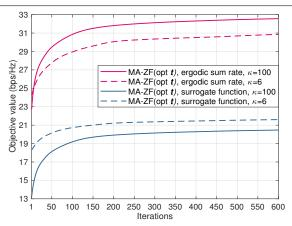


Fig. 4. The convergence of the proposed MA-ZF Algorithm 2. with power allocation (10), and the antenna positions are optimized via Algorithm 1, also using two-timescale CSI.

- 3) **FPA with ZF beamforming and power allocation**: "FPA-ZF (opt *p*)" uses ZF beamforming with optimized power allocation, leveraging instantaneous CSI.
- 4) FPA with MRT beamforming and power allocation: "FPA-MRT (opt p)", employs MRT beamforming with optimized power allocation based on instantaneous CSI.
- 5) FPA with optimal beamforming: "FPA-OPT (opt W)" applies optimal adaptive beamforming to the FPA system, using instantaneous CSI for performance comparison.

Figs. 3 and 4 show the convergence of the proposed MA-MRT (Algorithm 1) and MA-ZF (Algorithm 2) schemes with N=6, M=5. Both algorithms optimize surrogate functions to approximate the ergodic sum rate, with a predetermined fraction increase threshold $\zeta = 0.5 \times 10^{-4}$. Both algorithms exhibit efficient and stable convergence, where the ergodic sum rate increases steadily as iterations progress, especially under strong LoS conditions. MA-MRT converges within 450 iterations under both high ($\kappa = 100$) and moderate ($\kappa = 6$) Rician factors, with a minor gap between the surrogate and actual values. MA-ZF shows more steady and significant performance gains and typically converges within 500 iterations, with the surrogate function acting as a lower bound to the ergodic sum rate. These results demonstrate the effectiveness of the proposed methods in optimizing the ergodic sum rate under our proposed two-timescale framework.

Figs. 5 and 6 evaluate the ergodic sum rate performance of various schemes across different transmit power levels with $\kappa=100$ and $\kappa=6$, respectively. In both figures, MA-ZF consistently outperforms the other approaches across all transmit power levels except for the very low power scenario $P_{\text{tot}}=9dBm$, effectively exploiting spatial degrees of freedom provided by antenna repositioning. In contrast, MA-MRT exhibits a significantly lower ergodic sum rate compared to MA-ZF, highlighting the limitations of MRT beamforming in managing multiuser interference. A key observation is the impact of the Rician factor on system per-

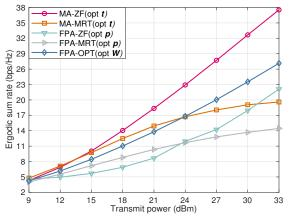


Fig. 5. Ergodic sum rate versus maximum transmit power with N=6, M=5 and $\kappa=100$.

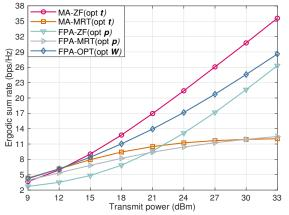


Fig. 6. Ergodic sum rate versus maximum transmit power with N=6, M=5 and $\kappa=6$

formance. As the Rician factor decreases from $\kappa=100$ to $\kappa=6$ transitioning from strong to weaker LoS conditions, there is a noticeable decline in performance for MA-enabled schemes, particularly MA-MRT, due to the reduced availability of deterministic channel components. Encouragingly, MA-ZF maintains robustness across both strong and moderate LoS scenarios. In summary, MA-enabled systems exhibit superior or comparable performance to FPA-based systems, with MA-ZF consistently outperforming MA-MRT. These results highlight the performance gains achieved by optimizing antenna positions, especially in strong LoS environments. Nonetheless, it is important to note that MAs alone cannot replace well-designed transmit beamforming; instead, they work in synergy with beamforming to maximize overall system performance.

For a clearer investigation into the impact of Rician factors, Figs. 7 and 8 depict the ergodic sum rate as a function of the Rician factor κ . Across all scenarios, MA-enabled schemes benefit significantly from increasing κ , aligning with expectations under the two-timescale design. As the channel becomes more deterministic, the optimization potential of the proposed scheme expands. Except in weak LoS conditions where $\kappa \leq 0$, MA-ZF consistently achieves the highest ergodic sum rate, even surpassing the performance of optimal beamforming. Remarkably, despite using equal power allocation and being a sub-optimal beamforming scheme, MA-ZF demonstrates the significant performance potential of MAs in moderate to strong LoS conditions, which underscores the importance of

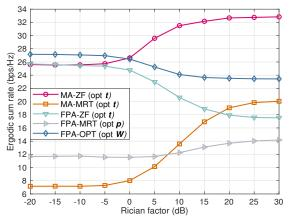


Fig. 7. Ergodic sum rate versus Rician factor with N=6, M=5.

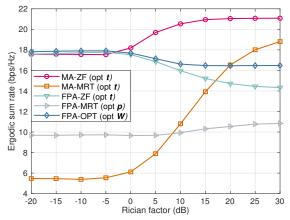


Fig. 8. Ergodic sum rate versus Rician factor with $N=4,\,M=3.$

wireless channel reshaping and fully exploiting spatial degrees of freedom enabled by MAs. MA-MRT also sees considerable improvement as κ increases, benefiting from stronger deterministic LoS components. When κ approaches 30 dB, MA-MRT reaches performance levels comparable to FPA-ZF and even FPA-OPT, especially with fewer users (N=4,M=3). However, MA-MRT remains inferior to MA-ZF across all values of κ , again highlighting the limitations of MRT beamforming in scenarios where interference suppression is crucial, such as systems with high user density (N=6,M=5).

Figs. 9 and 10 illustrate the impact of the movable region size A on the ergodic sum rate for the proposed schemes under different user-antenna configurations and Rician factors. As the region expands, both MA-ZF and MA-MRT benefit from increased flexibility in position tuning, leading to steady improvements in performance. However, the performance gains begin to taper off beyond a certain region size, especially for MA-ZF, indicating that further enlarging the region offers diminishing returns. This suggests that the algorithm may have already converged to a locally optimal solution, and additional spatial flexibility provides limited benefit. In contrast, MA-MRT continues to see more pronounced improvements as the region expands, particularly under higher Rician factors. This indicates that the MA-based scheme with MRT beamforming requires a larger movable region to effectively mitigate interference and optimize performance. In other words, these results also imply that MA-ZF can exploit channel variation and achieve near-optimal performance more efficiently with a

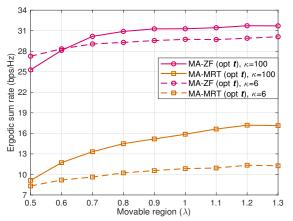


Fig. 9. Ergodic sum rate versus movable region size with N=6, M=5.

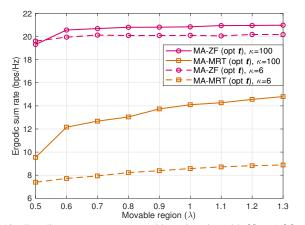


Fig. 10. Ergodic sum rate versus movable region size with N=4, M=3.

relatively smaller region, making it more effective for practical applications with constrained antenna movement.

Finally, Figs. 11 and 12 explore the relationship between the number of users M and the ergodic sum rate for various MA and FPA configurations under ZF and MRT beamforming, with N=6 and N=8, respectively. From both figures, it is observed that MA-ZF consistently delivers performance gains as the number of users increases, maintaining superiority over other schemes, particularly in scenarios with more users. In contrast, MA-MRT shows a gradual increase in performance but struggles with multiuser interference, leading to a decline in performance as the number of users approaches the number of antennas. Under high Rician factor conditions, MA-MRT achieves sum rates comparable to FPA-ZF and notably outperforms FPA-MRT. Given its low complexity, MA-MRT offers a promising alternative to sophisticated beamforming designs in FPA systems. In low Rician factor environments, the overall performance trends remain similar, but the rates drop due to the reduced deterministic LoS component, with MA-MRT being particularly impacted, rendering it almost ineffective. Despite this, MA-ZF continues to deliver superior performance as the number of users increases, showcasing its robustness in both strong and moderate LoS conditions. Moreover, comparing the results for N=6 and N=8, the addition of antennas boosts sum rates across all configurations, with the improvement being more pronounced for MA-ZF. This highlights MA-ZF's ability to leverage spatial diversity for effective multiuser interference management.

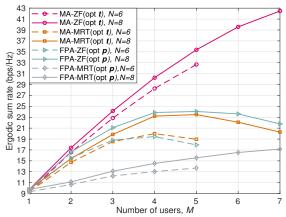


Fig. 11. Ergodic sum rate as a function of the number of users M for MA and FPA configurations N=6 and N=8 with $\kappa=100$.

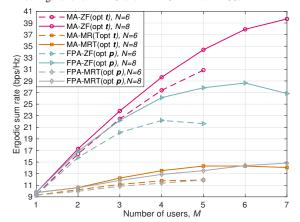


Fig. 12. Ergodic sum rate as a function of the number of users M for MA and FPA configurations N=6 and N=8 with $\kappa=6$.

VI. CONCLUSION

In this paper, we proposed a two-timescale transmission framework for MA-enabled MU-MIMO systems. The largetimescale optimization leverages statistical CSI to design optimal MA positions, maximizing long-term ergodic performance. In the small timescale, with MA positions fixed, MRT or ZF beamforming vectors are determined based on instantaneous CSI to adapt to short-term channel fluctuations. This decoupling of MA position optimization from the instantaneous transmission process provides a solution that strikes a balance between performance and practicality, effectively reducing the update frequency of MAs' positions and lowering channel estimation overhead. Within this framework, we developed position optimization algorithms for both MRT and ZF beamforming schemes. For MA with MRT, we proposed an AO and SCA-based algorithm that iteratively optimizes antenna positions, thereby refining the approximation of the ergodic sum rate. Similarly, for MA with ZF beamforming, we used AO, SCA, and MM techniques to iteratively maximize the ergodic sum rate through a lower-bound surrogate objective function. Extensive numerical results validated the effectiveness of the proposed two-timescale design, demonstrating significant gains in ergodic sum rate compared to conventional FPA systems. The results highlighted the superiority of MA with ZF beamforming, particularly in moderate LoS conditions and high user density. In contrast, MA with MRT beamforming offers a simplified alternative to more complex beamforming

designs in strong LoS conditions with moderate user density. Moreover, these findings indicate the synergy of combining beamforming and MA techniques for effective interference management.

Building upon the current two-timescale design, future research can further explore hierarchical or multi-timescale joint beamforming and antenna position optimization in MA-enabled systems. Specifically, by tailoring these adaptive optimizations to specific user densities, spatial distributions, and varying channel conditions or statistical characteristics, it is possible to develop more fine-grained, efficient, and practical system designs. These approaches could hold the potential to enhance the performance and practicality of the MA technique, thereby making MA-enabled MIMO systems a key solution for diverse next-generation wireless networks.

REFERENCES

- A. J. Paulraj, D. A. Gore, R. U. Nabar, and H. Bolcskei, "An overview of MIMO communications—A key to gigabit wireless," *Proc. IEEE*, vol. 92, no. 2, pp. 198–218, Feb. 2004.
- [2] G. L. Stüber, J. R. Barry, S. W. McLaughlin, Y. Li, M. A. Ingram, and T. G. Pratt, "Broadband MIMO-OFDM wireless communications," *Proc. IEEE*, vol. 92, no. 2, pp. 271–294, Feb. 2004.
- [3] D. Gesbert, M. Kountouris, R. W. Heath, C.-b. Chae, and T. Salzer, "Shifting the MIMO Paradigm," *IEEE Signal Process. Mag.*, vol. 24, no. 5, pp. 36-46, Sep. 2007.
- [4] E. G. Larsson, O. Edfors, F. Tufvesson, and T. L. Marzetta, "Massive MIMO for next generation wireless systems," *IEEE Commun. Mag.*, vol. 52, no. 2, pp. 186–195, Feb. 2014.
- [5] L. Lu, G. Y. Li, A. L. Swindlehurst, A. Ashikhmin, and R. Zhang, "An overview of massive MIMO: Benefits and challenges," *IEEE J. Sel. Topics Signal Process.*, vol. 8, no. 5, pp. 742–758, Oct. 2014.
- [6] I. F. Akyildiz, C. Han, Z. Hu, S. Nie, and J. M. Jornet, "Terahertz band communication: An old problem revisited and research directions for the next decade," *IEEE Trans. Commun.*, vol. 70, no. 6, pp. 4250–4285, June 2022.
- [7] F. Sohrabi and W. Yu, "Hybrid digital and analog beamforming design for large-scale antenna arrays," *IEEE J. Sel. Topics Signal Process.*, vol. 10, no. 3, pp. 501–513, Apr. 2016.
- [8] H. Zhang, S. Huang, C. Jiang, K. Long, V. C. M. Leung, and H. V. Poor, "Energy efficient user association and power allocation in millimeterwave-based ultra dense networks with energy harvesting base stations," *IEEE J. Sel. Areas Commun.*, vol. 35, no. 9, pp. 1936–1947, Sep. 2017.
- [9] Q. Wu and R. Zhang, "Towards smart and reconfigurable environment: Intelligent reflecting surface aided wireless network," *IEEE Commun. Mag.*, vol. 58, no. 1, pp. 106–112, Jan. 2020.
- [10] Q. Wu, S. Zhang, B. Zheng, C. You, and R. Zhang, "Intelligent reflecting surface-aided wireless communications: A tutorial," *IEEE Trans. Commun.*, vol. 69, no. 5, pp. 3313–3351, May 2021.
- [11] L. Zhu, W. Ma, and R. Zhang, "Movable antennas for wireless communication: Opportunities and challenges," *IEEE Commun. Mag.*, early access, Oct. 16, 2023, doi: 10.1109/mcom.001.2300212.
- [12] K.-K. Wong, A. Shojaeifard, K.-F. Tong, and Y. Zhang, "Fluid antenna systems," *IEEE Trans. Wireless Commun.*, vol. 20, no. 3, pp. 1950–1962, Mar. 2021.
- [13] K.-K. Wong and K.-F. Tong, "Fluid antenna multiple access," *IEEE Trans. Wireless Commun.*, vol. 21, no. 7, pp. 4801–4815, Jul. 2022.
- [14] L. Zhu, W. Ma, and R. Zhang, "Movable-antenna array enhanced beamforming: Achieving full array gain with null steering," *IEEE Commun. Lett.*, early access, Oct. 11, 2023, doi: 10.1109/lcomm.2023.3323656.
- [15] W. Ma, L. Zhu, and R. Zhang, "MIMO capacity characterization for movable antenna systems," *IEEE Trans. Wireless Commun.*, early access, Sep. 7, 2023, doi: 10.1109/TWC.2023.3307696.
- [16] L. Zhu, W. Ma, and R. Zhang, "Modeling and performance analysis for movable antenna enabled wireless communications," *IEEE Trans. Wireless Commun.*, early access, Nov. 14, 2023, doi: 10.1109/TWC.2023.3330887.
- [17] L. Zhu, W. Ma, B. Ning, and R. Zhang, "Movable-antenna enhanced multiuser communication via antenna position optimization," *IEEE Trans. Wireless Commun.*, early access, Dec. 12, 2023, doi: 10.1109/TWC.2023.3338626.

- [18] G. Hu, Q. Wu, K. Xu, J. Ouyang, J. Si, Y. Cai, and N. Al-Dhahir, "Movable-antenna array enabled multiuser uplink: A low-complexity gradient descent for total transmit power minimization," 2023, arXiv: 2312.05763. [Online]. Available: https://arxiv.org/abs/2312.05763
- [19] Z. Xiao, X. Pi, L. Zhu, X.-G. Xia, and R. Zhang, "Multiuser communications with movable-antenna base station: Joint antenna positioning, receive combining, and power control," 2023, arXiv: 2308.09512. [Online]. Available: https://arxiv.org/abs/2308.09512
- [20] Y. Zhang, Y. Zhang, L. Zhu, S. Xiao, W. Tang, Y. C. Eldar, and R. Zhang, "Movable antenna-aided hybrid beamforming for multiuser communications," 2024, arXiv: 2402.00123. [Online]. Available: https://arxiv.org/abs/2402.00123
- [21] H. Qin, W. Chen, Z. Li, Q. Wu, N. Cheng, and F. Chen, "Antenna positioning and beamforming design for fluid antenna-assisted multiuser downlink communications," *IEEE Wireless Commun. Lett.*, early access, Apr. 2024.
- [22] H. Wang, Q. Wu, and W. Chen, "Movable antenna enabled interference network: Joint antenna position and beamforming design," 2024, arXiv: 2403.13573. [Online]. Available: https://arxiv.org/abs/2403.13573
- [23] Y. Gao, Q. Wu, and W. Chen, "Joint transmitter and receiver design for movable antenna enhanced multicast communications," 2024, arXiv: 2404.11881. [Online]. Available: https://arxiv.org/abs/2404.11881
- [24] J. Ding, Z. Zhou, C. Wang, W. Li, L. Lin, and B. Jiao, "Secure full-duplex communication via movable antennas," 2023, arXiv: 2403.20025. [Online]. Available: https://arxiv.org/abs/2403.20025
- [25] L. Zhu, W. Ma, Z. Xiao, and R. Zhang, "Performance analysis and optimization for movable antenna aided wideband communications," 2024, arXiv: 2401.08974. [Online]. Available: https://arxiv.org/abs/2401.08974
- [26] W. Ma, L. Zhu, and R. Zhang, "Compressed sensing based channel estimation for movable antenna communications," *IEEE Commun. Lett.*, vol. 27, no. 10, pp. 2747–2751, Oct. 2023.
- [27] Z. Chai, K.-K. Wong, K.-F. Tong, Y. Chen, and Y. Zhang, "Port selection for fluid antenna systems," *IEEE Commun. Lett.*, vol. 26, no. 5, pp. 1180–1184, May 2022.
- [28] Y. Ye, L. You, J. Wang, H. Xu, K.-K. Wong, and X. Gao, "Fluid antennaassisted MIMO transmission exploiting statistical CSI," *IEEE Commun. Lett.*, vol. 28, no. 1, pp. 223–227, Jan. 2024.
- [29] X. Chen, B. Feng, Y. Wu, D. W. Kwan Ng and R. Schober, "Joint beamforming and antenna movement design for movable antenna systems nased on statistical CSI," in *Proc. IEEE Global Commun. Conf.* (GLOBECOM), Kuala Lumpur, Malaysia, 2023, pp. 4387-4392.
- [30] G. Hu, Q. Wu, D. Xu, K. Xu, J. Si, Y. Cai, N. Al-Dhahir, "Two-Timescale design for movable antenna array-enabled multiuser uplink communications," 2024, arXiv:2407.17841. [Online]. Available: https://doi.org/10.48550/arXiv.2407.17841
- [31] Z. Zheng, W. Jing, Z. Lu, Q. Wu, H. Zhang and D. Gesbert, "Cooperative Multi-Satellite and Multi-RIS Beamforming: Enhancing LEO SatCom and Mitigating LEO-GEO Intersystem Interference," in *IEEE J. Sel. Areas Commun.*, early access, Sep. 13, 2024, doi: 10.1109/JSAC.2024.3460068.
- [32] M.-M. Zhao, Q. Wu, M.-J. Zhao, and R. Zhang, "Intelligent reflecting surface enhanced wireless networks: Two-timescale beamforming optimization," *IEEE Trans. Wireless Commun.*, vol. 20, no. 1, pp. 2–17, Jan. 2021.
- [33] Q. Zhang, S. Jin, K.-K. Wong, H. Zhu, and M. Matthaiou, "Power scaling of uplink massive MIMO systems with arbitrary-rank channel means," *IEEE J. Sel. Topics Signal Process.*, vol. 8, no. 5, pp. 966–981, Oct. 2014.
- [34] Y. Zeng, Q. Wu, and R. Zhang, "Accessing from the sky: A tutorial on UAV communications for 5G and beyond," *Proc. IEEE*, vol. 107, no. 12, pp. 2327–2375, Dec. 2019.
- [35] Y. Sun, P. Babu and D. P. Palomar, "Majorization-minimization algorithms in signal processing, communications, and machine learning," IEEE Trans. Signal Process., vol. 65, no. 3, pp. 794-816, 1 Feb.1, 2017.
- [36] M. Grant and S. Boyd, "CVX: MATLAB software for disciplined convex programming," Accessed: 2016. [Online]. Available: http://cvxr.com/cvx
- [37] K. Wang, A. M.-C. So, and T.-H. Chang, "Outage constrained robust transmit optimization for multiuser MISO downlinks: Tractable approximations by conic optimization," *IEEE Trans. Signal Process.*, vol. 62, no. 21, pp. 5690–5705, Nov. 2014.
- [38] K. Zhi, C. Pan, H. Ren, and K. Wang, "Ergodic rate analysis of reconfigurable intelligent surface-aided massive MIMO systems with ZF detectors," *IEEE Commun. Lett.*, vol. 26, no. 2, pp. 264–268, Feb. 2022.
- [39] X. Yu, D. Xu, and R. Schober, "Enabling secure wireless communications via intelligent reflecting surfaces," in *Proc. IEEE Global Commun. Conf. (GLOBECOM)*, Waikoloa, HI, USA, 2019, pp. 1–6.